Nocturnal Chemistry in the Urban Boundary Layer of Los Angeles

Final Report
Contract No. 08-318

April 2012

Prepared for:
California Air Resources Board and
California Environmental Protection Agency

Prepared by:
Dr. Jochen Stutz
University of California, Los Angeles
7127 Math Sciences
Los Angeles, CA 90095

Disclaimer

The statements and conclusions in this Report are those of the contractor and not necessarily those of the California Air Resources Board. The mention of commercial products, their source, or their use in connection with material reported herein is not to be construed as actual or implied endorsement of such products.

Acknowledgements

Authors would like to thank the California Air Resources Board for providing funding for this project through contract # 08-318.

We also would like to thank our collaborators Barry Lefer and Christine Haman from the University of Houston for sharing the ceilometer data; Hans Osthoff and Levi Mielke from the University of Calgary for the $ClNO_2$ data, and NOAA for hydrocarbons and meteorological data.

We want to thank Professor John H. Seinfeld and the administration of the California Institute of Technology for their support and for hosting the CalNex-LA supersite on the campus grounds.

Many thanks go to Maria Valenzuela and Kelly Kitasato of the City of Pasadena, Real Property Office, Burt Tibbet of Magic Growers; Melvin Matthews and staff of the Kinneloa Irrigation District; and Chief Vidales, and Jose Martinez together with all other firefighters working at Henningers Flats for their support and cooperation in installing and maintaining the LP-DOAS retroreflectors during the CalNex experiment.

Lastly, we would like to thank Joost De Gouw of NOAA and Jose Jimenez of the University of Colorado – Boulder for their hard work as co-organizers of the CalNex-LA experiment.

The statements and conclusions in this Report are those of the contractor and not necessarily those of the California Air Resources Board. The mention of commercial products, their source, or their use in connection with material reported herein is not to be construed as actual or implied endorsement of such products.

Table of Contents

List of Figures

List of Tables

Abstract

The State of California continues to face air quality challenges in its major urban areas. Ozone and particulate matter (PM) levels in the South Coast Air Basin exceed the California and Federal standard regularly, and the ever growing population makes the development of further strategies to improve air quality a priority. To support the State's air pollution mitigation goals this project focused on the investigation of nocturnal chemistry in the Los Angeles basin. While often ignored, nocturnal chemistry is important, as the processes occurring at night set the stage for air quality conditions on the next day. To support other research efforts to better understand the processes underlying air pollution the University of California Los Angeles (UCLA) organized the CalNex Los Angeles supersite, which was located on the campus of the California Institute of Technology. The supersite, which hosted more than 40 research groups, yielded a highly comprehensive data set of gaseous and particulate pollutants and meteorological parameters from May 15, 2010 to June 16, 2010.

As part of Calnex-LA, UCLA's LP-DOAS instrument continuously measured vertical concentration profiles of O_3, NO_2, HCHO, SO_2, HONO and NO_3 in four altitude intervals: 33-78 m, 78-121 m, 121-255 m, and 255-556 m above the ground. This unique dataset was interpreted using a 1-dimensional chemistry and transport model to yield the following main conclusions:

- Nocturnal atmospheric composition and chemistry in Los Angeles is highly altitude dependent.
- The high levels of the dominant nocturnal radical species NO_3, in particular above 200 m altitude, showed that active nocturnal radical chemistry is occurring.
- Uptake of N_2O_5 on particles was found to be responsible for an altitude-averaged nocturnal loss of nitrogen oxides of 0.7 to 1.3 ppb/h. which is comparable to the daytime NO_x loss.
- N_2O_5 chemistry led to the efficient formation of $ClNO_2$, an important Cl atom precursor in the morning, which was observed by the collaborators from the University of Calgary.
- Nitrous acid, HONO, an important hydroxyl-radical precursor, showed elevated mixing ratios in the lowest 100 m of the atmosphere. Surface conversion of NO_2 to HONO on the ground was identified as the most likely source.
- Elevated daytime HONO mixing ratios show the presence of an active daytime HONO source. A photo-enhanced conversion of NO_2 on the ground was identified as the most likely HONO source.
- The photolysis of morning and daytime HONO was identified as a major contributor to the daytime primary radical budget, with a potentially large influence on ozone levels.

The results show that the nocturnal chemistry of nitrogen species strongly influences air quality in Los Angeles. Nighttime and daytime nitrous acid chemistry, which is currently poorly represented in urban air quality models, is an important contributor to the hydroxyl radical budget, thus impacting ozone chemistry. The data acquired in the project as well as the scientific conclusions from this project can be used to validate and improve models of the Los Angeles airshed and will thus lead to more accurate description of ozone and particle formation.

1 Executive Summary

Air quality in urban areas remains a serious environmental challenge in the State of California. Ozone and particulate matter (PM) levels in the South Coast Air Basin exceed the California and Federal standard regularly, and the ever growing population makes the development of further strategies to improve air quality a priority. To support the State's air pollution mitigation goals this project focused on the investigation of nocturnal chemistry in the Los Angeles basin. Understanding of nocturnal chemistry is important, as night-time hours set the stage for air quality conditions on the next day. In addition, University of California Los Angeles (UCLA) took the lead in organizing the CalNex Los Angeles supersite. The site, which was located on the campus of the California Institute of Technology, hosted more than 40 research groups that performed a highly comprehensive set of pollutant and meteorological measurements from May 15, 2010 to June 16, 2010. Most of the data acquired at the field site has been posted on a National Oceanic and Atmospheric Administration (NOAA) hosted web-site and is available to the California Air Resources Board.

UCLA deployed its longpath Differential Optical Absorption Spectroscopy (LP-DOAS) instrument on the Caltech campus to measure vertical profiles of O_3, NO_2, HCHO, SO_2, HONO and NO_3 during the CalNex-LA experiment. The data analysis produced vertical trace gas mixing ratios in four altitude intervals: 33-78 m, 78-121 m, 121-255 m, and 255-556 m above ground level. Vertical profiles of steady state N_2O_5 were also calculated. The data were interpreted with the help of UCLA's 1-D chemistry and transport model. The following main conclusions were derived:

- Nocturnal atmospheric composition and chemistry in Los Angeles is highly altitude dependent. The observed vertical profiles of O_3, NO_2, and NO_3, can be explained by surface emissions of NO and slow vertical mixing.

- Mixing ratios of NO_3 and N_2O_5 of over 150 ppt and 2 ppb, respectively, were observed. The highest mixing ratios were present above 200 m altitude. The observations are indicative of active nocturnal radical chemistry and the efficient formation of $ClNO_2$, which was observed by the collaborators from the University of Calgary.

- The average nocturnal NO_x loss in the lowest 550 m of the atmosphere was found to be between 0.7 and 1.3 ppb/h. This loss rate is comparable to the daytime NO_x loss due to OH chemistry. N_2O_5 aerosol uptake was identified as the main nocturnal NO_x loss pathway.

- Observed nocturnal vertical profiles of HONO show elevated mixing ratios predominately in the lowest 50-100 m of the atmosphere, followed by a fast decay with altitude. The profiles could be reproduced with UCLA's 1-D model through a parameterization of the surface conversion of NO_2 to HONO.

- Daytime HONO mixing ratios exceeded those expected from a photo-stationary state between OH, NO and HONO, indicating an active daytime HONO source. Hourly averaged daytime vertical HONO profiles and the diurnal profile of the $HONO/NO_2$ ratio point to a photo-enhanced conversion of NO_2 on the ground as the dominant HONO source.

- The morning photolysis of HONO accumulated during the night is an important early morning OH source at the surface. However, due to the strong vertical gradient of HONO, its importance is diminished if the entire column of the lower atmosphere is considered. The OH formation rate from daytime HONO photolysis can be similar to that of ozone photolysis. This process can thus considerably influence daytime ozone chemistry.

The results show that the nocturnal chemistry of nitrogen species can strongly influence air quality in Los Angeles. The observation of daytime HONO and its contribution to the OH budget also illustrates the importance of HONO chemistry during the day. The conclusions from this project can be used to validate and improve models of the Los Angeles airshed and will thus lead to more accurate description of ozone and particle formation.

2 Introduction

California has a long history as the world leader in the development of successful air quality regulatory programs. Much of California's success in reducing air pollution can be attributed to strategies that are based on a sound scientific understanding of the processes leading to elevated levels of gaseous and particulate air pollutants. Despite the progress made over the past six decades, pollution remains a problem in many Californian cities, and in particular in the South Coast Air Basin. In support of the State's goal to better understand how to control ozone and PM pollution, this project is aimed at elucidating an important aspect of the atmospheric chemistry of California's large urban centers that has not been sufficiently studied: *The mechanisms of nocturnal air pollution chemistry and their impact on daytime ozone and aerosol concentrations.*

The lack of solar radiation at night causes a considerable change in the chemical processes of the urban atmosphere. Hydroxy radical levels are typically low and the nitrate radical, NO_3, is the most important radical species. NO_3 reacts rapidly with a number of hydrocarbons, leading to their removal from the atmosphere. Even more important is the impact of NO_3 chemistry on the budget of nitrogen oxides. NO_3 can directly react with particles, leading to a destruction of one NO_x and one ozone molecule. It is also in equilibrium with NO_2 and N_2O_5. The latter is known to be efficiently taken up on particles, leading to a loss of NO_x and an increase in particulate nitrate. While the chemical pathways of these reactions are known, considerable uncertainty exists about their impact on air quality in the urban atmosphere. For example, the true atmospheric uptake coefficients of NO_3 and N_2O_5 are poorly known, thus leading to uncertainties in the NOx budget. The impact of heterogeneous reactions on the urban canopy and vertical transport also introduce considerable uncertainties in our understanding of nocturnal air pollution chemistry.

Another important nighttime (and most likely also daytime) specie is nitrous acid, HONO. The photolysis of HONO is an important source of OH radicals in the morning. There are indications that HONO contributes significantly to the daytime OH budget. The sources of HONO in the atmosphere are still very uncertain. It is clear that HONO originates from the heterogeneous conversion of NO_2 on surfaces, i.e. the ground, buildings and the aerosol. Which of these surfaces plays the most important role is still unclear, as is the exact chemical mechanism converting NO_2 to HONO in the urban atmosphere. Consequently urban airshed models are incomplete in their description of HONO chemistry, often calculating nocturnal (and daytime) concentrations far less than those observed. This introduces considerable uncertainties in the model, in particular in the hydroxyl radical budget, which need to be resolved to further improve the predictions of smog formation.

An additional challenge in describing nocturnal chemistry is the suppression of vertical mixing due to the radiative cooling of the ground at night. This can lead to an accumulation of pollutants emitted near the ground, and thus to strong gradients in the vertical profiles of all trace gases and their chemistry. Routine air monitoring stations and even the more highly instrumented ground sites are incapable of providing information on the vertical variation in concentrations, which is thus not well quantified.

Nocturnal chemistry in urban areas is one of the most poorly studied aspects of urban air pollution. Many urban airshed models have not been thoroughly evaluated for nocturnal conditions, and those that have often perform rather poorly. Many of these problems stem from a

lack of field observations that sufficiently describe the chemistry and meteorology in cities at night. This project was motivated by a desire to improve our understanding of nocturnal processes to provide a better description of the chemistry and transport at night in chemical models of urban air. The specific goals of this project were:

- To provide, for the first time in the Los Angeles Basin, direct observations of the vertical profiles of the most important nocturnal trace gases, O_3, NO_2, NO_3, steady state N_2O_5,and HONO, as well as other gases, i.e. HCHO, SO_2, throughout the nights, the morning, and the day.
- To quantify the ozone and NO_x budget at night and determine the NO_3 and N_2O_5 aerosol uptake coefficients in Los Angeles using our observations and calculations with our 1-D chemical transport model.
- To study the impact of HONO chemistry on the HO_x radical budget by determining the OH formation rates from its photolysis, and compare them to that of other OH sources. The comparison of the observations and 1-D chemical transport model calculations will be used to shed light on the processes forming HONO in urban areas, which are represented poorly in current air quality models.

The following report will describe our activities over the past three years. As part of these activities, and as a service to the atmospheric chemistry community and the State of California, we also took the lead in organizing the Los Angeles surface site during the 2010 CalNex experiment. The report will begin with a short review of nocturnal NO_3 and HONO chemistry. In Chapter 3 the CalNex-LA field site and the measurements assembled during the CalNex-LA experiment will be briefly described. Chapter 4 provides the details regarding the methods we employed in pursuit of our research goals. Chapter 5 summarizes the results from our field efforts. Chapter 6 and 7 describe our results with regard to NO_3 chemistry / nocturnal NO_x budget and HONO chemistry, respectively. The report will end with a discussion of our results and how they relate to the questions we set out to answer in this project.

2.1 Nocturnal Radical Chemistry / NO_x Budget

The daytime formation of pollutants such as ozone and aerosols is driven by the chemistry of HO_x (OH + HO_2) radicals. This chemistry is strongly interwoven with that of reactive nitrogen species, in particular NO and NO_2 (=NO_x). The level of NO_x is one of the factors determining ozone formation efficiency and OH radical levels. NO_x chemistry is also closely linked to ozone chemistry through a cycle that continually inter-converts O_3, NO_2 and NO during the day.

$$NO + O_3 \rightarrow NO_2 + O_2 \quad (2.1)$$

$$NO_2 + h\nu \rightarrow NO + O \quad (2.2)$$

$$O + O_2 \rightarrow O_3 \quad (2.3)$$

Because reactions 2.1 – 2.3 form a null-cycle with respect to ozone, ozone formation occurs through reactions which convert NO into NO_2 without using O_3, such as:

$$NO + HO_2\bullet \rightarrow NO_2 + OH\bullet \quad (2.4)$$

During the day the primary sources of OH/HO_2 radicals are the photolysis of O_3, HCHO and HONO and, to a smaller extent, the reaction of ozone with alkenes. OH chemistry is also responsible for a large portion of urban aerosol formation through the oxidation of volatile organic carbons to low vapor pressure particle precursor species. To accurately quantify ozone and particle formation it is crucial to understand the budgets of HO_x and the factors influencing it, such as the budgets of NO_x, VOCs, and the various OH precursors.

In an urban area the NO_x budget during the day is dominated by direct emissions as the main source and the conversion of NO_2 to nitric acid as the main loss pathway:

$$OH\bullet + NO_2 \rightarrow HNO_3 \quad (2.5)$$

This reaction also removes HO_x radicals and is responsible for decreasing ozone formation efficiency at the high NO_x concentrations, as often observed in highly polluted areas.

Since OH is formed predominately through the photolysis of various precursor species its concentration at night is typically low. Thus Reaction 2.5 plays only a minor role in removing NO_x from the system. Nevertheless, up to 30 – 50% of NO_x in a 24 hour period can be removed at night through the chemistry of the nitrate radical, NO_3, which together with ozone assumes the role of the dominant oxidant at night.

The source of NO_3 in the troposphere is the relatively slow reaction of NO_2 with ozone [*Wayne et al.*, 1991]:

$$NO_2 + O_3 \rightarrow NO_3 + O_2 \quad (2.6)$$

The formation rate of NO_3, $P(NO_3)$, is thus proportional to the concentrations of ozone and NO_2:

$$P(NO_3) = k_{O3+NO2} \times [O_3] \times [NO_2] \quad (2.7)$$

A number of sinks for NO_3 are known. During the day NO_3 is rapidly photolyzed.

$$NO_3 + h\nu \rightarrow NO_2 + O \quad (2.8)$$

$$NO_3 + h\nu \rightarrow NO + O_2 \quad (2.9)$$

The branching ratio between reactions 2.8 and 2.9 is typically around 0.9, therefore favoring reaction 2.8. Reactions 2.6 and 2.8 together with the reaction of the O atom with O_2 form a null-cycle, while the path through Reaction 2.9 destroys ozone via Reaction 2.1. Another important NO_3 removal process is NO_3 reaction with NO:

$$NO_3 + NO \rightarrow 2\ NO_2 \quad (2.10)$$

with a loss rate of:

$$f_{NO3}(NO) = k_{NO+NO3} \times [NO] \quad (2.11)$$

NO_3 photolysis and its reaction with NO decrease NO_3 levels sufficiently that its chemistry is often of minor importance during the day, although certain daytime reactions may still be significant [*Geyer et al.*, 2003; *Osthoff et al.*, 2006].

Reaction 2.10 is also important in nocturnal environments with direct NO sources. Particularly in urban areas with direct NO emissions from traffic, this reaction can control the

NO_3 concentrations at night. Since most NO sources are located at the surface, the importance of this reaction depends on the vertical mixing of NO and the competing reaction of NO with ozone. It should be noted that Reaction 2.10 does not truly impact the NO_x or ozone budgets, but rather converts ozone into NO_2, which can then be photolyzed again to NO and O_3 in the morning.

NO_3 also reacts rapidly with unsaturated hydrocarbons. This reaction proceeds mainly via the addition of the NO_3 radical to the carbon double bond, forming organic nitrates.

$$NO_3 + R1\text{-}C{=}C\text{-}R2 \rightarrow R1\text{-}C\text{-}C(NO_3)\text{-}R2 \quad (2.12)$$

The overall loss rate of NO_3 through the reactions with hydrocarbons can be quantified by:

$$f_{NO3}(HC) = \sum_j k_j \times [HC_j] \quad (2.13)$$

NO_3 can also be taken up on aerosol particles [*Docherty and Ziemann*, 2006; *Karagulian and Rossi*, 2007; *Mak et al.*, 2007], but the uptake coefficients are not well known. Overall, all reactions of NO_3, except that with NO and its photolysis, lead to the removal of a NO_x molecule at night [*Dentener and Crutzen*, 1993; *Geyer and Stutz*, 2004; *Stutz et al.*, 2004b, *Brown et al.*, 2003, 2004].

The often dominant pathway of NO_x removal at night proceeds through the uptake of N_2O_5 onto the aerosol. N_2O_5 is in equilibrium with NO_2 and NO_3 at night:

$$NO_2 + NO_3 + M \leftrightarrow N_2O_5 + M \quad (2.14)$$

N_2O_5 is efficiently taken up on particles forming aerosol nitrate.

$$N_2O_5 + H_2O(s) \rightarrow 2\ HNO_3\ (solid) \quad (2.15)$$

If the particles contain chloride, Cl^-, the uptake of N_2O_5 can also lead to the formation of gas-phase $ClNO_2$. This was directly observed in Houston by *Osthoff et al.*, (2008). $ClNO_2$ is photolyzed in the morning to:

$$ClNO_2 + h\nu \rightarrow Cl + NO_2 \quad (2.16)$$

thus releasing one of the NO_x molecules lost through the N_2O_5 uptake. More importantly, the Cl atom is a strong oxidizer, being able to jumpstart photochemistry in the morning.

A number of laboratory and field studies have determined uptake coefficients for N_2O_5 on aerosol. The reported uptake coefficients vary from ~0.07 on pure ammonium bisulfate particles at high R.H., 0.005 for soot [*Mak et al.*, 2007], to values down to 0.001 and below for organic particles [*Thornton et al.*, 2003]. *Kane et al.* (2001) also showed that the uptake coefficient on

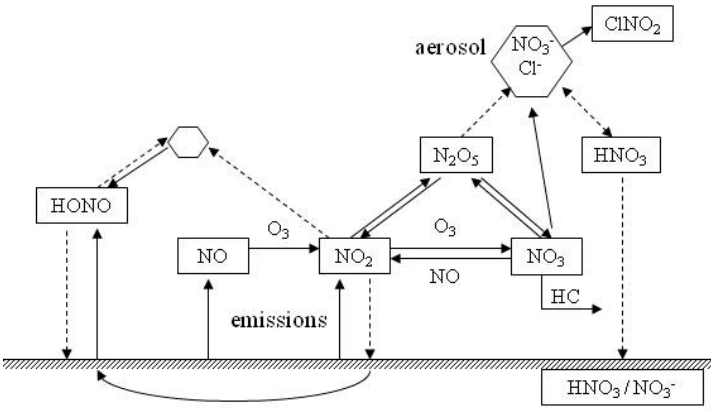

Figure 2.1: Schematic of the dominant nocturnal NO_x reactions.

ammonium sulfate varies from 0.042 at high R.H. to 0.001 at low R.H., while the uptake coefficient on ammonium bisulfate varies with R.H. between 0.69 and 0.015. Recently, *Bertram and Thornton* (2009) published a parameterization for the N_2O_5 uptake coefficient and the yield of $ClNO_2$. In short, the uptake coefficient and yield depend on the amount of nitrate and chloride in the particle as well as on particulate water, which is often related to relative humidity. The N_2O_5 uptake coefficient can also be impacted by coating of organic material on the particle [*Thornton and Abbatt*, 2005]. This was confirmed by *Brown et al* (2006) who extracted reactive uptake coefficients from their aircraft observations in the range of 0.017 to below 0.001, showing the variability of this parameter in the atmosphere.

Figure 2.1 shows an overview of the most significant NO_x reactions at night. Based on the known reactions it is possible to set up an equation for the steady state NO_3 and N_2O_5 concentrations [*Geyer and Stutz,* 2004]. The steady state NO_3 concentration is determined by its formation rate, i.e. the rate of the $O_3 + NO_2$ reaction, and its steady state lifetime τ_{NO3}:

$$[NO_3] = k_8 \cdot [NO_2] \cdot [O_3] \cdot \tau_{NO3} \tag{2.17}$$

The steady state concentration of N_2O_5 on the other hand is determined by its equilibrium with NO_3, NO_2 and N_2O_5 and its loss rate:

$$[N_2O_5] = \frac{k_{NO2+NO3\rightarrow N2O5}[NO_3][NO_2]}{k_{N2O5\rightarrow NO2+NO3} + f_{N2O5}} \tag{2.18}$$

It should be noted that under warmer summer conditions in mid-latitudes the N_2O_5 loss frequency is often much smaller that its thermal decay. The steady state N_2O_5 concentration is thus most often calculated omitting the loss frequency f_{N2O5}. *Geyer and Stutz* (2004) also showed that Eq. 2.17 – 2.18 are altitude dependent and that vertical transport of N_2O_5 should be included in Eq. 2.18. While the steady state approach to determine NO_3 and N_2O_5 is only an approximation due to the short chemical lifetimes of these species, the approximation is quite good in urban areas.

Few observations of NO_3 in polluted urban areas have been reported. *Platt and Perner* (1980), were the first to show the presence of NO_3 in Los Angeles. A number of other studies confirmed these observations, finding NO_3 mixing ratios exceeding 300 ppt in Los Angeles [*Harris et al.*, 1983; *Platt et al.*, 1984; *Mackay* 1994]. In recent years our group has published a number of observations showing the presence of 50 – 200 ppt above 50 m altitude in the urban areas of Houston and Phoenix [*Stutz et al*, 2004a; *Wang et al.*, 2006, *Stutz et al.*, 2010]. These studies also showed the strong altitude dependence of NO_3 levels, i.e. negligible levels near the surface and a maximum in the upper part of the NBL.

The poorly constrained N_2O_5 uptake coefficients and $ClNO_2$ yields make it challenging to accurately quantify the NO_x budget at night. Another problem in determining the NO_x budget is the strong vertical variability of the N_2O_5 profile [*Geyer and Stutz,* 2004; *Stutz et al.*, 2004b, *Brown et al.*, 2007a,b], which makes it necessary to integrate over the vertical extent of the atmosphere to derive values which are significant for the overall budget. *Geyer and Stutz* (2004) and *Stutz et al.* (2004b) for example, found that the rates of various ozone and NO_x loss processes at 3 and 10 m were considerably different from those averaged over the lowest 100 m of the atmosphere.

2.2 Chemistry of HONO

Nitrous acid, HONO, has long been known as a precursor of OH radicals in urban atmospheres. Since the first identification of HONO in Los Angeles by *Perner and Platt* (1979), the photolysis of HONO

$$HONO + h\nu \rightarrow OH + NO \quad (2.19)$$

has been known to be the primary source of OH in the early morning in urban areas, with diurnally averaged contributions to the OH budget of up to 34% near the ground [*Alicke et al.*, 2002, 2003; *Aumont et al.*, 2003]. Consequently HONO formation and photolysis can impact ozone formation [*Aumont et al.*, 2003; *Harris et al.*, 1982; *Jenkin et al.*, 1988; *Ren et al.*, 2006] and the oxidation of various pollutants, as well as the formation of aerosol through the oxidation of SO_2 , NO_2, and various hydrocarbons [*Aumont et al.*, 2003].

Despite its importance for outdoor and indoor air quality, the details of HONO formation remain poorly known. Laboratory studies showed that HONO is formed through first order conversion of NO_2 on surfaces with adsorbed water [*Finlayson- Pitts et al.*, 2003; *Jenkin et al.*, 1988; *Kleffmann et al.*, 1998; *Pitts et al.*, 1984b; *Sakamaki et al.*, 1983; *Svensson et al.*, 1987]. Because the HONO yield is close to 50%, and the remaining nitrogen is found as surface adsorbed HNO_3 [*Goodman et al.*, 1999; *Kleffmann et al.*, 1998; *Svensson et al.*, 1987], the following stoichiometry has been proposed as a qualitative description of HONO formation:

$$NO_2 + NO_2 + H_2O \rightarrow HONO + HNO_3 \quad (2.20)$$

HONO formation mechanisms involving NO [*Calvert et al.*, 1994; *Saliba et al.*, 2000; *Sjödin and Ferm*, 1985], or soot particles [*Ammann et al.*, 1998], seem to play only a minor role in the atmosphere [*Gerecke et al.*, 1998; *Kalberer et al.*, 1999]. In one of the few studies that are more relevant to urban surfaces, *Kurtenbach et al.* (2001) determined the NO_2-HONO conversion frequency on a concrete traffic tunnel wall with a surface to volume ratio of 1 m^{-1} to be 5×10^{-5} s^{-1}. The formation of HONO in various combustion processes is also insufficient to explain mixing ratios of several ppbv observed in urban areas [*Kirchstetter et al.*, 1996; *Kurtenbach et al.*, 2001; *Pitts et al.*, 1984a].

In recent years observations of HONO above the expected photo-stationary state between reaction 2.19 and the gas-phase formation of HONO

$$OH + NO \rightarrow HONO \quad (2.21)$$

have been reported for various environments [*Acker et al.*, 2006a; *Acker et al.*, 2006b; *Acker and Moller*, 2007; *Kleffmann et al.*, 2006, *Wong et al.*, 2011b]. To explain these observations a number of new photo-enhanced reactions have been proposed [*Kleffmann*, 2007]. For example, the photolysis of surface adsorbed nitrate or nitric acid is believed to be the main source of HONO in polar and rural regions [*Zhou et al.*, 2002; *Grannas et al.*, 2007]. More recently, photo-enhanced NO_2 reduction on surface adsorbed organic impurities has been shown to form HONO [*Stemmler et al.*, 2007]. *Li et al.* (2008) also showed that HONO can be formed upon the gas-phase reaction of electronically excited NO_2, due to photoexitation, with water.

Over the years various field experiments have shown that HONO is always present in urban areas (see for example the review by *Lammel and Cape* (1996)). Nocturnal levels of HONO have been measured in the Los Angeles air basin at levels of 0 – 15 ppb [*Harris et al.*, 1982; *Platt and Perner*, 1980; *Winer and Biermann*, 1994; *Mackay* 1994]. While these measurements were performed many years ago, they show that HONO is important in the South Coast Basin. A number of more recent studies have shown elevated HONO levels of up to 3 ppb in other US cities [*Stutz et al.*, 2004a, *Wong et al.*, 2011a].

While there is growing evidence for the significance of HONO in the urban environment, our understanding of HONO formation and its impact on ozone and particle formation is incomplete. Most studies to date have only considered HONO photolysis close to the surface, ignoring the fact that HONO shows strong vertical gradients at night and even sometimes during the day [*Wong et al.*, 2011b]. The formation mechanism of HONO is unclear, making it challenging to incorporate its chemistry into any model. Finally, the true levels of HONO during the day remain uncertain, due to possible artifacts in chemical techniques to measure HONO. It is thus crucial to perform observations of the vertical distribution of HONO and to further investigate HONO levels during the day.

3 The CalNex - LA Experiment

The CalNex experiment was a large multi-platform and multi-location experiment. In addition to research vessels and research aircrafts, two main ground sites were set up: one in Bakersfield and one in the Los Angeles area.

As part of our activities our research group took the lead in organizing the Los Angeles ground site, which was located on the campus of the California Institute of Technology (Caltech), approximately 11 miles northeast of downtown Los Angeles at an elevation of 760ft above sea level (Figure 3.1).

Together with our collaborators Joost deGouw, NOAA, Jose Jimenez, CU Boulder, Jason Surrat and John Seinfeld, Caltech, we were able to put together an extremely comprehensive field site that measured a large number of gas-phase species, physical and chemical characteristics of aerosol, and meteorology. Tables 3.1 – 3.4 give an overview of the CalNex-LA participants, their instruments, and the parameters measured. The tables shows that a comprehensive set of gas-phase measurements was assembled, including state-of-the-art research grade instruments for various radical species (OH, HO_2, NO_3), a complete suite of nitrogen species (NO_x, NO_y, NO_3, N_2O_5, HONO, PANs, $ClNO_2$, HNO_3, aerosol nitrate), organics (VOCs, HCHO, CHOCHO, etc.), ozone, CO, CO_2, actinic fluxes, etc. A large number of aerosol instruments were also deployed, with many prototype instruments that were used for the first time in the field. Fourteen high volume aerosol samplers were also operated. In addition, we put together a relatively comprehensive suite of meteorological measurements including various surface meteorological stations, turbulent momentum and heat fluxes, and a ceilometer. The ceilometer, which was rented throughout this project, was one of the crucial support instruments as it allowed the direct measurement of the boundary layer height (BLH) using aerosol backscatter and its gradient at the boundary layer top (see *Haman et al*, (2012) for details on the ceilometer and its accuracy in determining BLH).

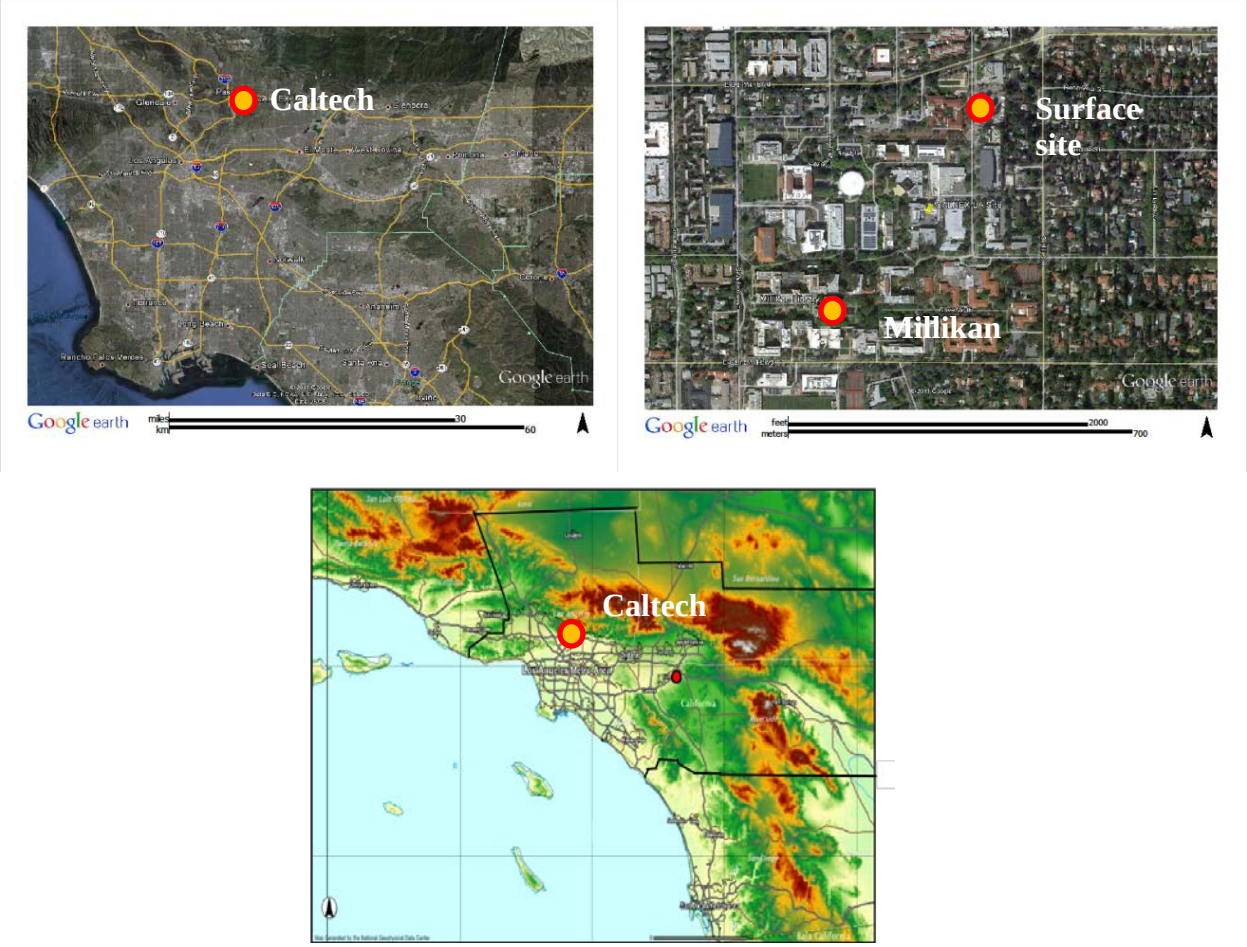

Figure 3.1: Google Map of the Los Angeles basin (left top), campus of California Institute of Technology (right top) with the locations of CalNex-LA site and Millikan Library marked. The bottom graph shows the CalNex-LA site in relation to the topography in southern California.

In total, close to 40 research groups participated in the Los Angeles field site and the number of researchers at the Caltech site reached up to 70-80 during certain times of the experiment. All of the involved researchers appreciate the ARB's additional funding for our project, which allowed UCLA to pay for the field site setup. It should be noted that many participants came with little or no budget, and were only able to participate due to the available infrastructure.

Many of the CalNex-LA measurements were used in this project. However, the scientific outcome of the project goes far beyond our project and one can expect a large number of scientific publications resulting from the CalNex-LA field site. The field site gave the most detailed insight to date into the gas-phase and aerosol chemistry in a large urban area.

Table 3.1: Overview of the CalNex-LA gas-phase measurements

O_3, NO_2, SO_2, NO_3, HONO, HCHO	DOAS	UCLA
OH and HO_2, OH reactivity	LIF – FAGE	Indiana Univ.
Photolysis frequencies, total sky imager	Scanning Actinic Flux Spectroradiometer	Univ. of Houston
O_3, SO_2, NO/NO_x, NO_y, CO	UV Abs / Flour/ CL+ photolysis cell and Mo converter / VUV	Univ. of Houston
Organic acids, HONO, HNCO, HCl , HNO_3	CIMS	NOAA
HCHO	Hantzsch reaction fluorescence	Univ. of Houston
CHOCHO, HONO, NO_2	CEAS	NOAA
PANs	GC-ECD	NOAA
$ClNO_2$, PANs	CIMS	U. Calgary
CO / CO_2	VUV / NDIR absorption	NOAA
Gas phase and semivolatile organics	High-resolution PTR-TOF MS	U. Utrecht
Water-soluble OC in the gas-phase	PILS and mist chamber + online WSOC	Georgia Tech
Total gas-phase organics & semivolatiles	High Resolution EI-TOF-MS	MIT
Gas-phase semivolatiles	Sorbent tubes + off-line TD-GCMS	CMU
Urban meteorology, eddy covariance	Various	NOAA ARL
HCHO, CHOCHO, NO_2, aerosol SCD	MAX-DOAS	CU Boulder
NH_3	QC-TILDAS	Univ. of Toronto
Soluble gases (HNO_3, NH_3)	GP-IC	CARB
$^{13}CO_2$	WS-CRDS	Caltech
Organic acids + other organics	MOVI-TOF-CIMS	Univ. of Washington
Daily canister for VOC analysis	Offline GC- FID / MS	US EPA Research
CHOCHO, NO_2	LED-CE-DOAS	CU Boulder
Met parameters	Ground site Caltech Library Roof	NOAA / Caltech
HONO	Wet Chemical (HPLC)	Univ. Paris
Semivolatile gas-phase hydrocarbons	Solid adsorption and liquid extraction	Loyola Marymount

Table 3.2: Overview of the CalNex-LA measurements of aerosol chemical and physical properties

	PAM	U-Boulder & Penn State
Organic aerosol composition	Soft-Ionization HR-ToF-AMS	CU Boulder
	TSI SMPS	CU Boulder
SO_4	Research-quality monitor	CARB
	TSI Water CPC 3786	CU Boulder
Particle number distrib.(300 nm - 10 um)	Grimm OPC 1.109	CU Boulder
OC and EC	1 hr Sunset Labs thermal-optical analyzer	Georgia Tech
Water-soluble OC in Particles	PILS and mist chamber + online WSOC	Georgia Tech
	PILS + ion chromatography and CIMS	Georgia Tech
1-hr molecular tracers (particles and semivol.)	TAG-AMS	UC Berkeley, Aer. Dynamics, Aerodyne, CU-Boulder
1-hr molecular tracers (part. & semivol.)	2D Thermal-Desorption Aerosol GC-MS (TAG)	UC Berkeley, Aer. Dynamics
PM semivolatile and non-volatile organics	High-resolution PTR-TOF MS	U. Utrecht
HR-MS analysis of WSOC/N compounds	PILS-collector + Electrospray-Orbitrap UHR MS	DOE PNNL EMSL
Black carbon & coating Composition	SP-AMS	U. Manchester, UK
	7-Wavelength Aethalometer	U. Manchester, UK
Black carbon absorption	DMT 3-Wavelength Photoacoustic Sensor	U. Manchester, UK
Black carbon mass	DMT SP2 (Soot Particle Soot Photometer)	U. Manchester, UK
Single particle composition 200-5000nm	PALMS	NOAA
	NAMS	U. Delaware
Cloud condensation nuclei (CCN) spectrum	DMT CCN Counter	Brookhaven NL
	SMPS + DMT CCN	Brookhaven NL
Ions in aerosol (SO_4, NO_3, Cl, K, etc.)	GP-IC	CARB
	MOVI-TOF-CIMS	Univ. of Washington
Submicron particle number distributions	TSI SMPS #2	CU Boulder
	UHSAS	CU Boulder
Supermicron size distribution & PBAP	UV-APS	CU Boulder

Table 3.3: Overview of the CalNex-LA aerosol optical properties

Aerosol LIDAR	3-wavelength LIDAR	USFS
Column aerosol optical depth	Sunphotometry / AERONET Station	UCLA
Aerosol extinction, scattering, albedo	CRDS / integrating sphere nephelometry	TTU
Boundary layer backscatter & height	Vaisala Ceilometer	Univ. Houston / UCLA

Table 3.4: Overview of the CalNex-LA aerosol sampler measurements

Organosulfates and nitrooxy organosulfates	Caltech/UNC
OOA characterization	University of York, UK)\
	PSI, Switzerland
	PSI, Switzerland
	US EPA Research
Compound-Specific Stable Isotope Analysis for SOA characterization and	
	US EPA Research
	UC Davis
	ASU
	Georgia tech
	CMU

3.1 CalNex-LA Site Organization

The instruments and samplers were placed on the Caltech campus at three locations. The main site was on a vacant lot on the north-east corner of the Caltech campus. To provide laboratory space eight office containers were rented and arranged around two sampling scaffolding towers (Figure 3.2). In addition, NOAA brought a mobile trailer to the site increasing the number of laboratory trailers to nine. The sampling towers were used to elevate many gas-phase instruments and sampling lines to about 10 m above the ground (see Figure 3.2). Three larger office containers and two storage containers for the shipping crates were also rented and placed on the lot. Caltech provided the laboratory and office trailers with power and internet connections. The aerosol high volume samplers and the NOAA-ARL surface meteorological station were located on the roof of the Keck Building on the Caltech campus (Figure 3.3).

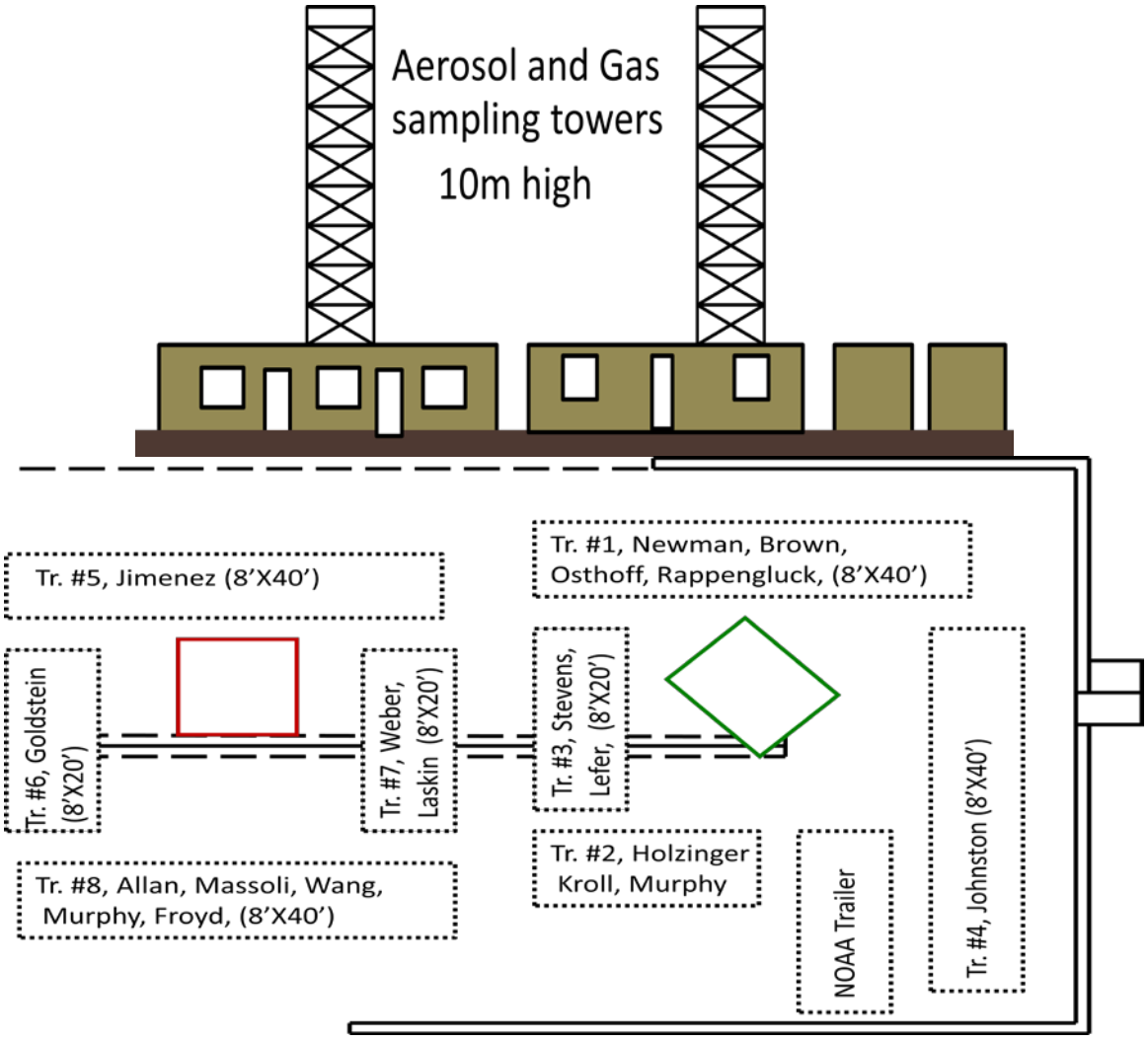

Figure 3.2: Sketch of the CalNex-LA surface site. Nine laboratory trailers were arranged around two 10 m high sampling towers (red: aerosol, green: gases).

In addition, UCLA's LP DOAS and CU-Boulder's MAX-DOAS and CEAS-DOAS instruments were placed on the roof of Caltech's Millikan Library. The placement of UCLA LP-DOAS instrument atop of one of the tallest buildings in the area provided a clear view between Caltech and a hillside further north where four retroreflectors were placed (see Chapter 4). The setup of the LA field site went smoothly and no major issues were encountered.

Figure 3.3: Photographs of the CalNex-LA site during the experiment. The top photograph shows the main surface site. The high-volume samplers on the Keck Building roof are shown in the lower left. Millikan Library and the LP-DOAS light beam are shown in the lower right.

3.2 Overview of CalNex LA Period

While it is beyond the scope of this report to analyze the environmental conditions during the CalNex-LA experiment, Figures 3.4 and 3.5 give an overview of the meteorological and air quality conditions during the sampling period from May 15 to June 15, 2010.

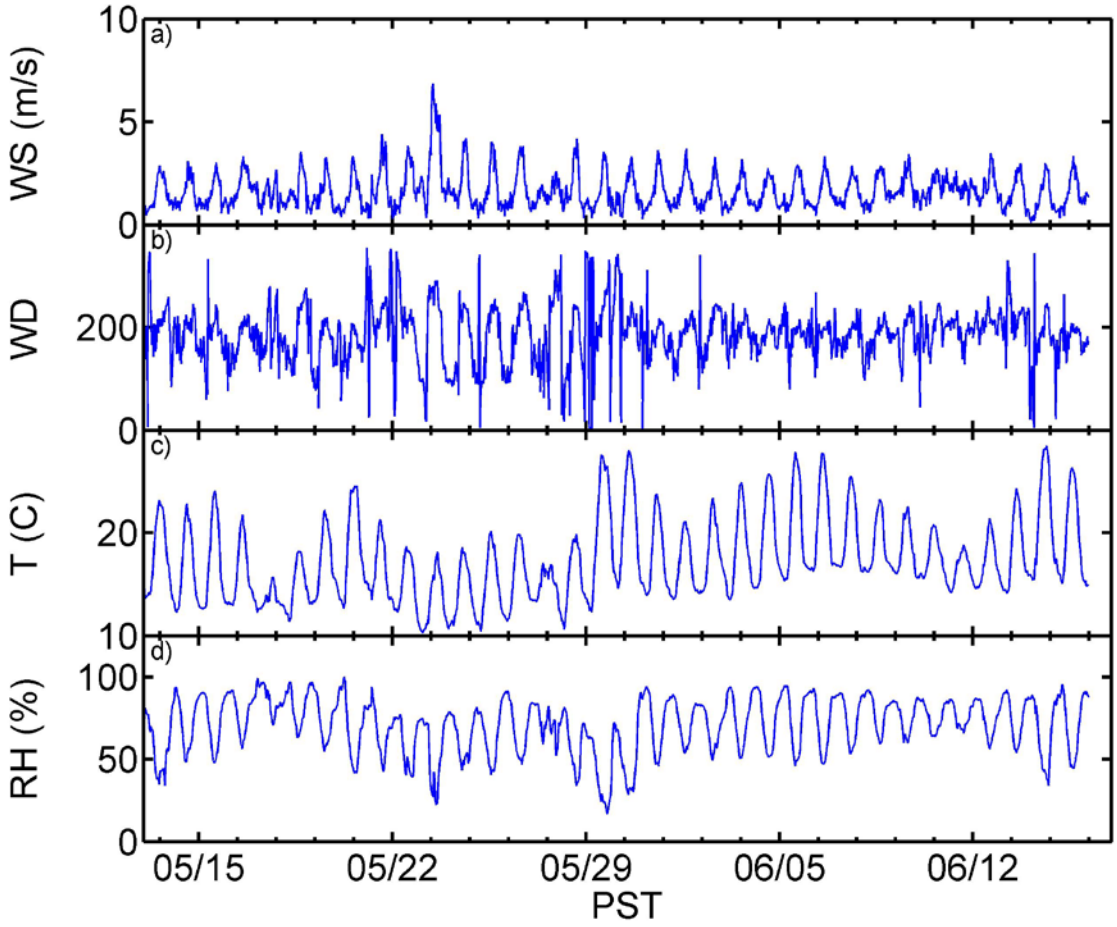

Figure 3.4: Meteorological data during the CalNex-LA experiment (courtesy of NOAA ARL). Tick marks in this figure, and all other figures in the report, are at midnight PST.

Meteorological conditions varied widely over the four week period. Lowest temperatures were found at night (down to 10°C) while the maximum temperatures during the day reached close to 30°C. Wind speeds were modest except for May 23, when a frontal system passed through southern California, also bringing rain. The Caltech site typically encountered modest winds from the coast during the day and weak winds at night, with some down slope flows from the nearby mountains. Relative humidity at night was often close to 100% and low (<500 m agl) clouds were common during much of the experiment.

Air pollutant data (Figure 3.5) shows that the first and last days of the experiment were somewhat polluted, while the period from 5/23 to 5/30 was relatively clean. A pollution episode was encountered from 6/3 to 6/10, as indicated by the elevated ozone and aerosol extinction values. These periods are also clearly reflected in the BLH determined by the ceilometer. During the polluted period BLH was around 700 m, while it was considerably higher during the cleaner period after 5/23. The CalNex-LA experiment thus covered a variety of meteorological

conditions that offer the opportunity to study ozone and aerosol chemistry under both relatively clean and polluted conditions.

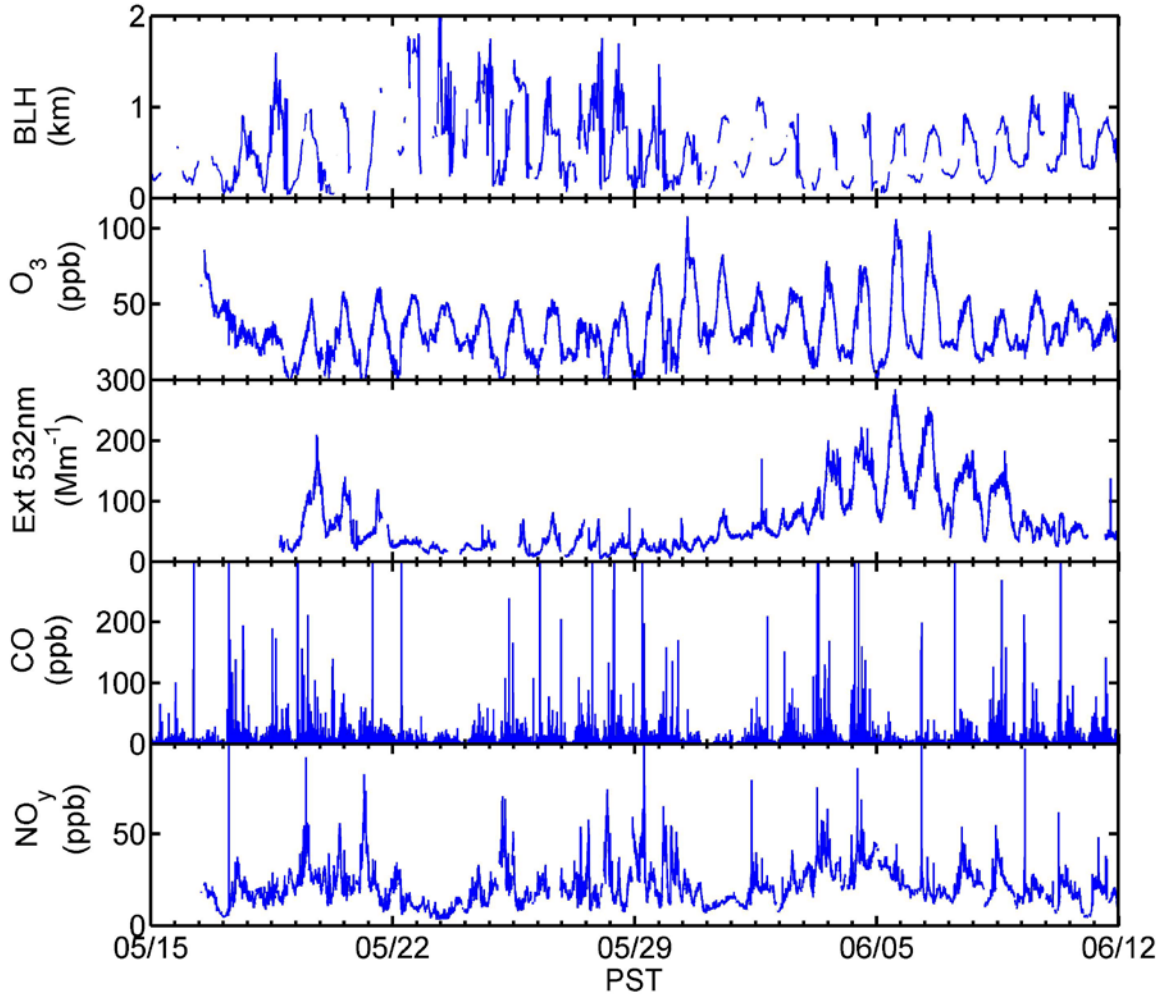

Figure 3.5: Main pollutants, aerosol extinction , and boundary layer height during the CalNex-LA experiment (courtesy of Univ. Houston, NOAA, and Aerodyne Inc.). The spikes in the CO and NOy data are from local emission at the CalNex-LA site, and are not completely displayed in the figure to improve the visibility of the overall data set.

3.3 Spatial Representativeness / Local Influences

An interesting question for any field experiment is how representative the surface in-situ measurements are for the area of the measurements. It is not uncommon for in-situ data to be influenced by local emissions that can skew the interpretation of the results. The combination of instruments at the CalNex-LA site allows a look into this question by comparing results from the in-situ observations with those from the longpath-DOAS (LP DOAS) instrument, which averages

over a several kilometers area (see Chapter 4 for details). The agreement between the two different systems during the day, and in the case of SO_2 also during the night, shows that ground site measurements were not impacted by local emissions, and that it is representative for an area of > 5 km around the site. Please note that the disagreement between the O_3 and NO_2 measurements at night is due to the vertical profiles of these species which will be discussed in Chapter 5.

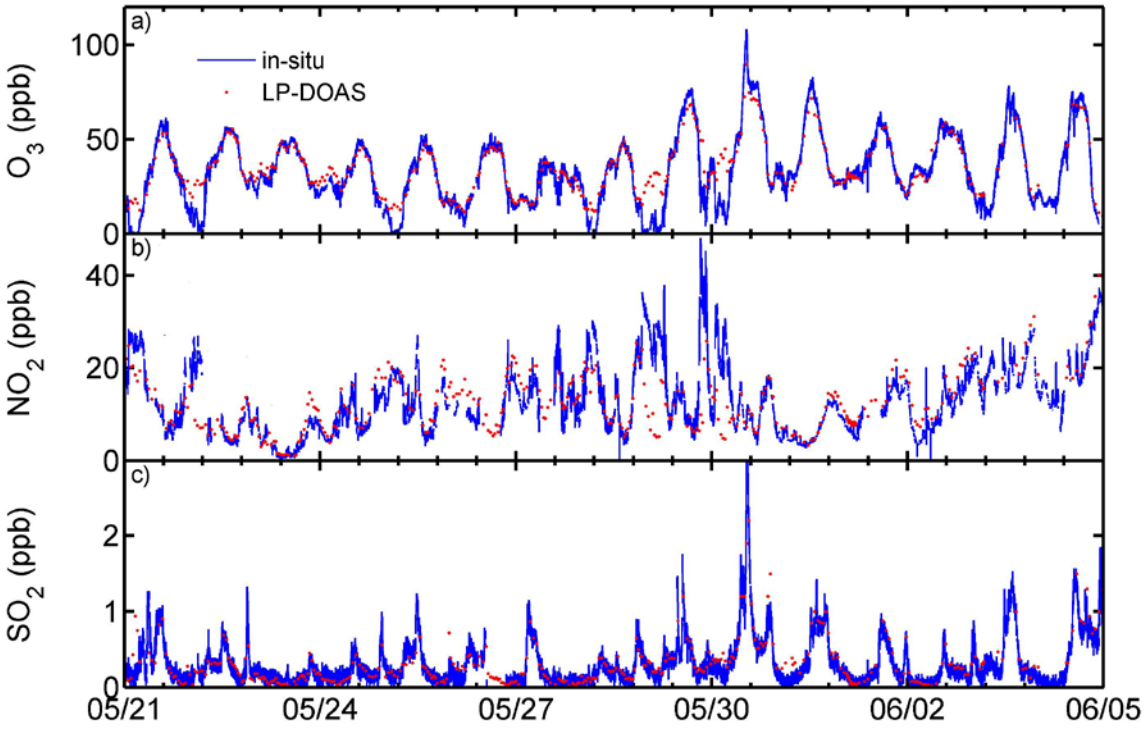

Figure 3.6: Comparison of in-situ observations at 10m altitude at the CalNex-LA surface site compared with those from the lowest LP-DOAS lightpath, which determined the average mixing ratios between the Millikan Library roof and the mountains at 5.4 km distance.

4 Experimental Methods and Modeling

Our group pursued the scientific goals described above by deploying a Long-Path Differential Optical Absorption Spectrometer (LP-DOAS) at Caltech to measure various trace gases in four height intervals from May 15 to June 15, 2010 on the east side of the Los Angeles urban area. These vertical profiles were interpreted using a 1-D chemistry and transport model. In this chapter we will give a description of the instrument setup and the methodology of the measurements. The 1-D model will also be briefly described.

4.1 Experimental Setup

The LP-DOAS was set up on the roof of the Millikan Library on the campus of the California Institute of Technology at 35 m above ground level (agl). Four retroreflector arrays were mounted about 5-7 km North-East of the instrument at 78 m, 121 m, 255 m and 556 m above the reference ground level at Caltech on the side of the San Gabriel mountains (Figure 4.1). A side view of the LP-DOAS setup during CalNex-LA, is shown in Figure 4.2.

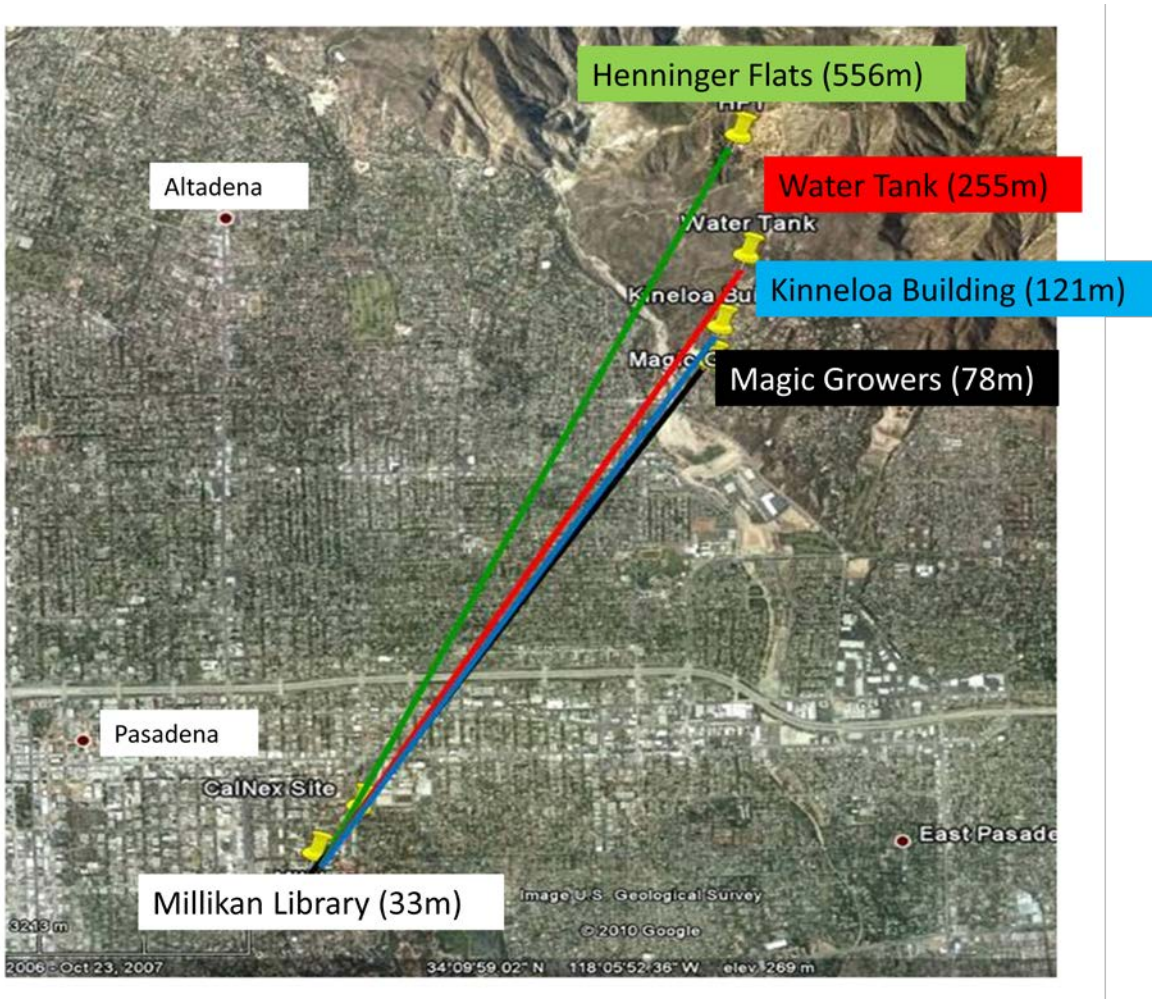

Figure 4.1: Aerial view of the LP-DOAS light paths. Elevations of retroreflector sites are in meters above the ground.

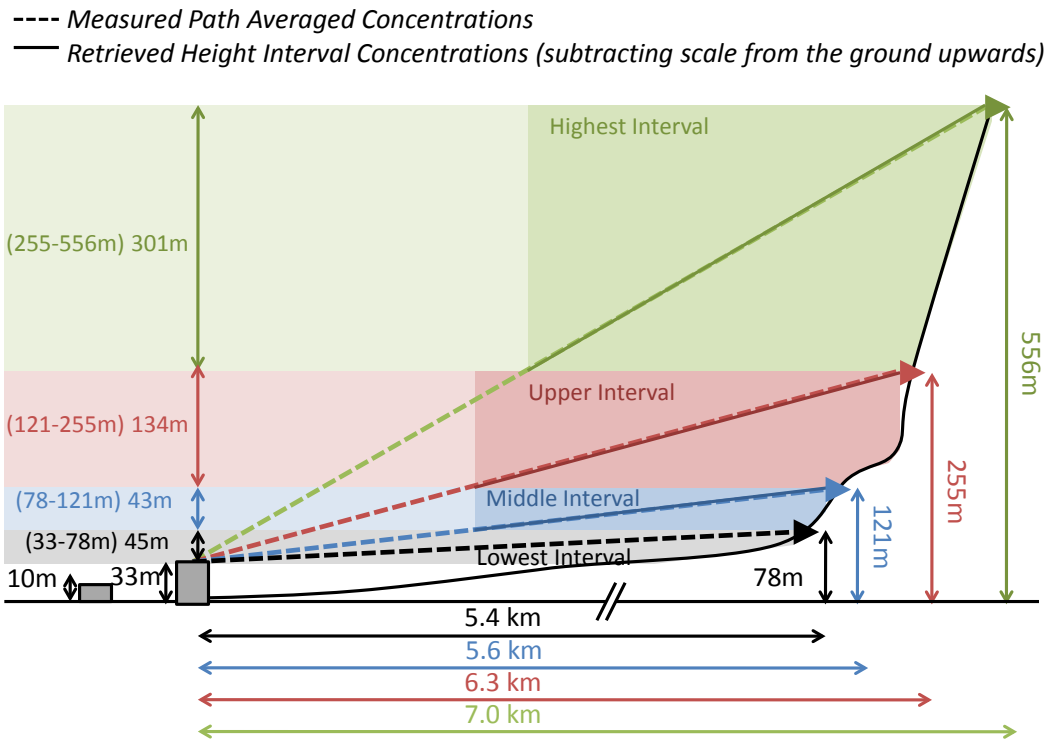

Figure 4.2: Side view of the LP-DOAS setup during CalNex. The figure also illustrates the geometric retrieval employed to convert the path-averaged data to mixing ratios averaged over the four altitude intervals. The colors of the height intervals will be used in the plots shown in this study.

The LP-DOAS instrument measured sequentially in three different wavelength ranges: 300-380 nm (for retrieval of O_3, SO_2, NO_2, HONO and HCHO); 400-460 nm (for retrieval of NO_2 and glyoxal); and 600-680 nm (for retrieval of NO_3) on all four light paths. For each wavelength range, information of the respective trace gases is recorded simultaneously. Therefore, even though all trace gases mentioned above are retrieved for each light path, only three measurements are performed for each light path. The measurements were performed continuously throughout the experiment. However, low clouds and fog sometimes blocked the light-paths. The upper light paths thus have gaps in the data coverage. Please note that we will use the color coding in Figure 4.2 for the remainder of this report.

4.2 Spectral Data Analysis

Analysis of the atmospheric absorption spectra was achieved using established DOAS methods using a combination of a linear and non-linear least squares fit of the known trace gas absorption features [*Platt and Stutz*, 2008]. Spectral absorption structures were incorporated in the fitting procedure using the literature absorption cross sections of O_3 [*Voigt et al.*, 2001], NO_2 [*Voigt et al.*, 2002], HONO [*Stutz et al., 2000*], HCHO [*Meller and Moortgat*, 2000], SO_2 [*Vandaele et al.*, 1994], and NO_3 [*Yokelson et al.*, 1994]. Errors of reported mixing ratios are calculated as 1σ statistical uncertainties by the analysis procedure for each individual spectrum and trace gas. The systematic error of the reported trace gas mixing ratios are dominated by the

uncertainties of the absorption cross sections of the respective trace gases which are in the range of 3 – 8%. The systematic error of the DOAS spectrometer was <3% [*Platt and Stutz*, 2008].

4.3 LP-DOAS Performance

The error of LP-DOAS measurements is calculated for each spectrum and trace gas. The errors thus vary with time and are reported as such. To give an overview of the instrument performance we list here the average and the best detection limits (calculated as twice the average and the best mixing ratio error). During times of good visibility errors of the measurements were smaller than during the times of poor visibility. Therefore, for times of good visibility the detection limits were close or equal to the best reported in Table 4.1. During times of low visibility the detection limits were sometimes elevated, leading to the higher values than the average detection limit in Table 4.1. In general, the LP-DOAS detection limits during CalNex-LA were better than those from previous campaigns, because of a series of improvements in the instrument, i.e. a new detector, and the underlying methodology.

Table 4.1: Detection limits of the LP-DOAS instrument during CalNex-LA

	Detection Limit average / best (ppb)			
Light Path	**Lower**	**Middle**	**Upper**	**Highest**
O_3	1.7 / 0.4	1.7 /0.4	1.8 / 0.6	2.1 / 0.5
NO_2	0.13 / 0.03	0.12 / 0.02	0.11 / 0.02	0.11 / 0.02
HONO	0.047 / 0.01	0.045/ 0.092	0.043 / 0.007	0.04 / 0.008
HCHO	0.35 / 0.1	0.34 / 0.1	0.31 / 0.1	0.29 / 0.07
SO_2	0.05 / 0.02	0.05 0.02	0.05 / 0.02	0.06 / 0.015
NO_3 (in ppt)	2.3 / 0.6	2.3/0.7	2.4/0.7	2.7/0.7

4.4 Vertical Profile Retrieval

In order to study the vertical distribution of the observed trace gases, the measured path averaged mixing ratios were converted to height interval averaged mixing ratios through a two step process. First, all mixing ratios were linearly interpolated onto the time grid of the lowest light path observations to account for the temporal variations originated by taking the measurements sequentially. The interpolations were made under the assumption that the change of trace gas mixing ratios between the times of the scans could be approximated using a linear function. In a second step, the path averaged mixing ratios for the upper three light paths were converted to height interval averaged mixing ratios by using equation 4.1.

$$c_i = \frac{(h_i - H)}{(h_i - h_{i-1})} S_i - \frac{(h_{i-1} - H)}{(h_i - h_{i-1})} S_{i-1} \quad (4.1)$$

Where H is the base height of the lowest light path (33 m), c is the retrieved mixing ratio, h is the top height (m), and S is the average mixing ratio of the i^{th} (middle, upper, highest) light path.

The mixing ratio along the lowest light path is the average mixing ratio for the lowest height interval.

The mixing ratios shown in the remainder of the report are the averaged mixing ratios and corresponding propagated uncertainties over four altitude intervals: lower (33-78 m), middle (78-121 m), upper (121-255 m), and highest (255-556 m). The original measurement errors were propagated to derive the uncertainties of the retrieved mixing ratios for each data point.

4.5 1-D Chemistry and Transport Model

The interpretation of vertical trace gas profiles is often difficult as they are simultaneously influenced by chemistry, emissions, and mixing. A tool that has proven to give unique insights into this complex system is UCLA's one-dimensional (1-D) Radical Chemistry and Transport model (RCAT). RCAT is a vertically highly resolved 1-D chemistry and transport model that was described in detail by *Geyer and Stutz* (2004). It includes the gas-phase Regional Atmospheric Chemistry Mechanism (RACM II) [*Stockwell et al.*, 1997], heterogeneous chemistry on the aerosol and ground, temporally varying biogenic emissions at the ground between 1m and 12m altitude; and anthropogenic emissions, predominately from traffic at 0.5m altitude. Photolysis frequencies are calculated according to *Landgraf and Crutzen* (1998). Calculations of heterogeneous chemistry on the ground and on the aerosol are included as well. The model subdivides the lowest 1 km of the atmosphere into 22 boxes (center of boxes at (m): 5×10^{-5}, 5.5×10^{-4}, 0.0055, 0.055, 0.55, 2, 4.5, 8, 15, 27.5, 42.5, 57.5, 72.5, 90, 112.5, 137.5, 162.5, 187.5, 225, 375, 625, 875, 2000). Box heights increase logarithmically below 1 m because vertical transport is less efficient near the surface. The upper border of the model currently extends from 1 km to 3 km, and is considered as the free troposphere above the nocturnal residual layer at night or the daytime convective boundary layer.

The model contains a number of unique features:

- The vertical transport of reactive trace gases is treated separately from that of unreactive gases, i.e. vertical transport is corrected for the effect of simultaneous chemistry [*Geyer and Stutz*, 2004].
- In contrast to most other chemistry and transport models, chemistry at the ground is treated explicitly, i.e. using reactive uptake coefficients and collision frequencies.

The model has been used both for sensitivity studies and to interpret field observations of vertical profiles [*Geyer and Stutz*, 2004, *Stutz et al.*, 2004b, *Wong et al.*, 2011a].

As part of our activities in this project we have expanded this model to include halogen chemistry, and in particular the formation of $ClNO_2$ from N_2O_5 uptake on the aerosol. While this was not part of our original proposal, the scientific understanding of nocturnal chemistry has evolved in the past few years. This expansion of the model was necessary to correctly calculate the nocturnal NO_x budget.

In this project the model is primarily used to aid in the interpretation of the field observations. We use an approach in which the trace gas mixing ratios averaged over the height of the LP-DOAS data are calculated from the model output and then compared with the observations. Using an iterative process we then adjust poorly constrained parameters, such as the NO emission rate, vertical transport, and NO_3 and N_2O_5 uptake, to match the model to the observations of O_3, NO_2, and NO_3 (see *Wong et al.* 2011a) for details on this approach). We also

consider meteorological data for the optimization, whenever available. Once this adjustment has been made we then proceed to interpret the various chemical cycles in the model, and in particular the height distribution of the various NO_3 reactions (see Chapter 6). We also used the model to test whether we understand the basic mechanisms of HONO formation (Chapter 7).

As described above (see also *Geyer and Stutz*, (2004)) nocturnal vertical profiles of trace gases, and in particular ozone and NO_2, mainly depend on two factors: vertical mixing and NO_x emission rates. Both parameters are often not known well enough to allow a detailed interpretation of our observations. Consequently, we iteratively adjust hourly emission rates and vertical mixing (by varying the Monin-Obukhov length) with the goal to best describe the observed vertical profiles of NO_2 and O_3. The sensitivity studies by *Wong et al.*, (2011a) show that this approach is typically successful, and that the profiles are quite sensitive to the adjustments of the two parameters.

5 Results

Measurements with UCLA's LP-DOAS system were performed from May 15 – June 16, 2010. During the first 4 days of the experiment the instrument was only operated on the lowest light path, as the other retroreflectors were still being set up. Starting on May 19, the instrument operated on all four light-paths, whenever visibility allowed. The trace gas mixing ratios in all four height intervals during the entire field experiment are shown in Figure 5.1.

This data has been made available to the CalNex collaborators and the colleagues at the ARB through a NOAA operated web-site:
http://esrl.noaa.gov/csd/tropchem/2010calnex/Ground/DataDownload/.

While the LP-DOAS operated continuously, during certain times low clouds and fog blocked some, if not all of the light paths. Nevertheless a fairly complete dataset was derived, allowing us to answer the scientific questions posed in our project. Ozone mixing ratios measured by the LP-DOAS during CalNex-LA ranged from near zero up to ~100 ppb. The lowest NO_2 mixing ratios were observed in the upper height interval and were at times close to 1 ppb. The highest NO_2 levels of up to 40 ppb were typically found at night in the lowest height interval. It should be noted that NO_2 levels by the in-situ monitors were sometimes even larger at the surface site. We will discuss the O_3 and NO_2 diurnal behavior in more detail below.

Formaldehyde, HCHO, was in the range of 1 ppb during the cleaner period of the CalNex-LA study. During the more polluted second half of the experiment, HCHO followed the diurnal profile of ozone, reaching maximum levels, often above 5 ppb, in the early afternoon. The highest HCHO was observed on 5/30/10 and was partly associated with a polluted air parcel or plume arriving at the CalNex-LA site (see Figure 5.2). This plume also contained the highest mixing ratios of SO_2 (~2 ppb). During most of the days, SO_2 mixing ratios were below 0.5 ppb. Only during certain events did SO_2 exceed this value. The origin of these events is currently not clear. NO_3 mixing ratios were below the detection limit during the day, but reached mixing ratios above 150 ppt during several nights. NO_3 was highest in the upper height interval, as will be discussed in Chapter 6. HONO levels ranged from 20 ppt during the day to 1.5 ppb at night and will be further discussed in Chapter 7.

To better discuss the general behavior of the various trace gases we will focus on a one week period during CalNex-LA (Figure 5.2).

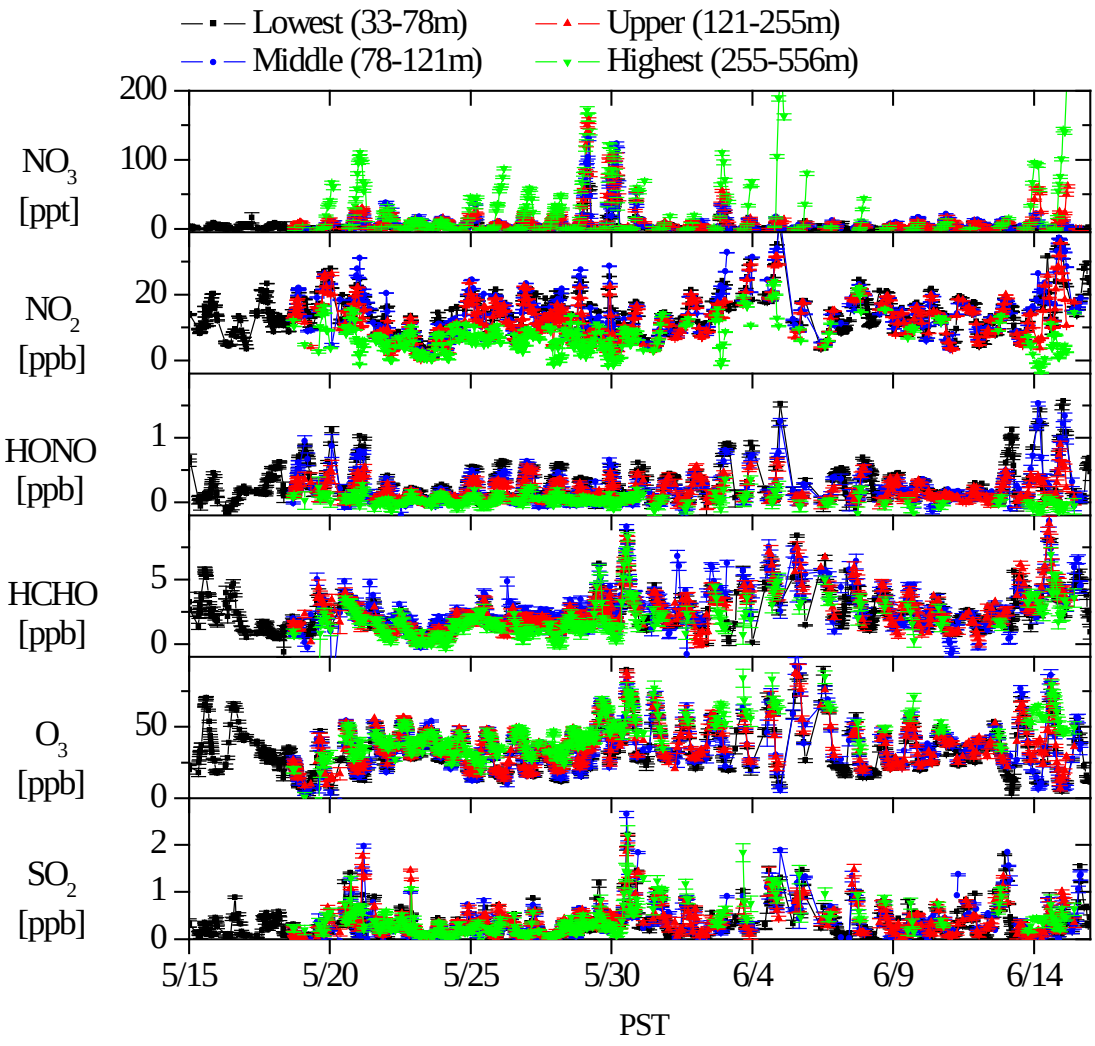

Figure 5.1: LP-DOAS data during CalNex-LA.

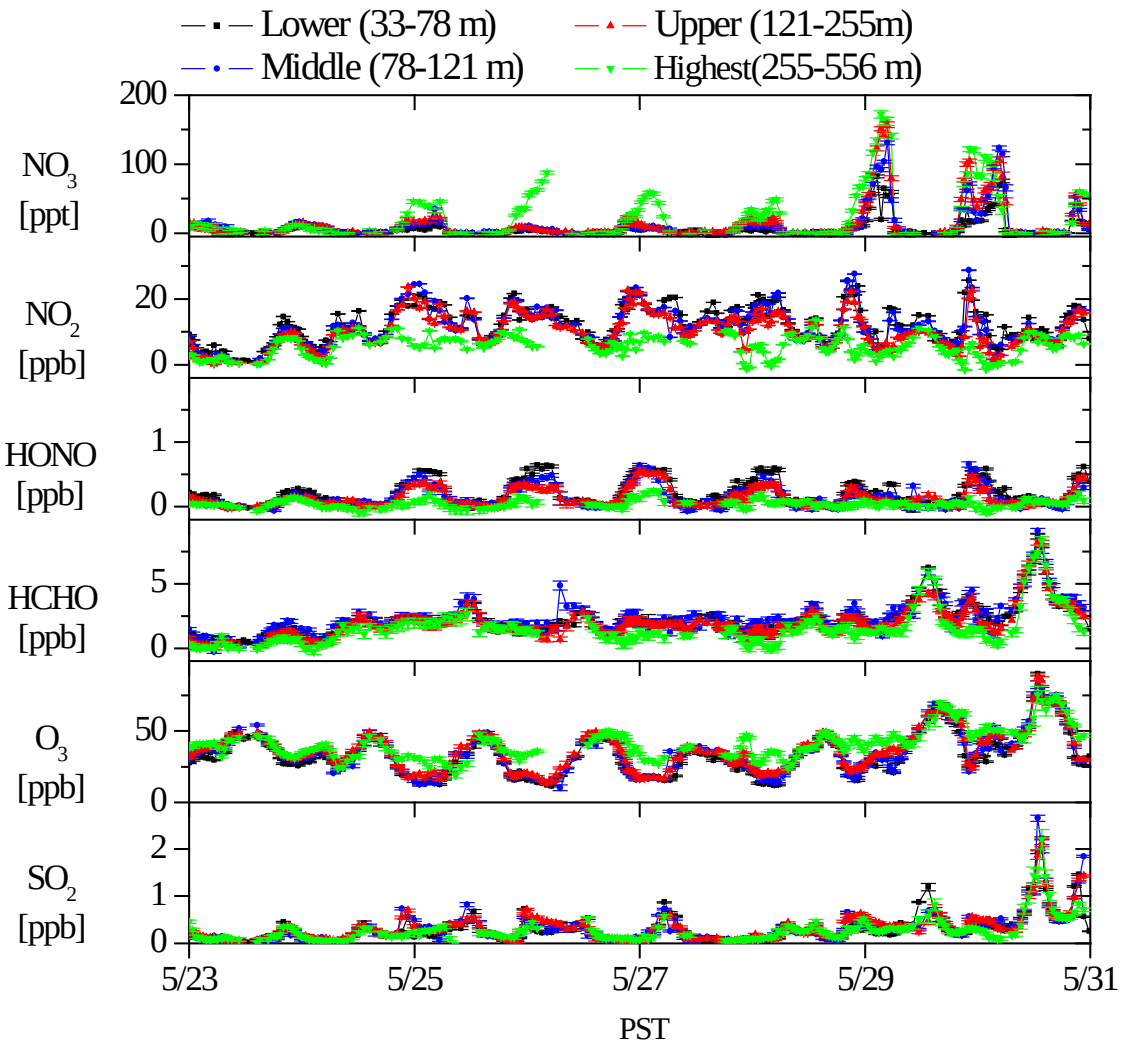

Figure 5.2: One week of vertical trace gas profiles retrieved from the LP-DOAS data during CalNex. The same color coding as in Figures 4.2 and 5.1 was used to distinguish the different height intervals.

The retrieved vertical profiles during this week show a slow buildup of O_3 and HCHO toward the end of the week, with highest levels on May 30th of ~90 ppb of O_3 and 8 ppb of HCHO at noon. Ozone shows the typical diurnal profile with lower values at night and higher values during the day. This behavior is more pronounced in the lower height intervals than in the highest interval. NO_2 shows the opposite behavior to ozone, with lower nocturnal values aloft and higher values near the surface.

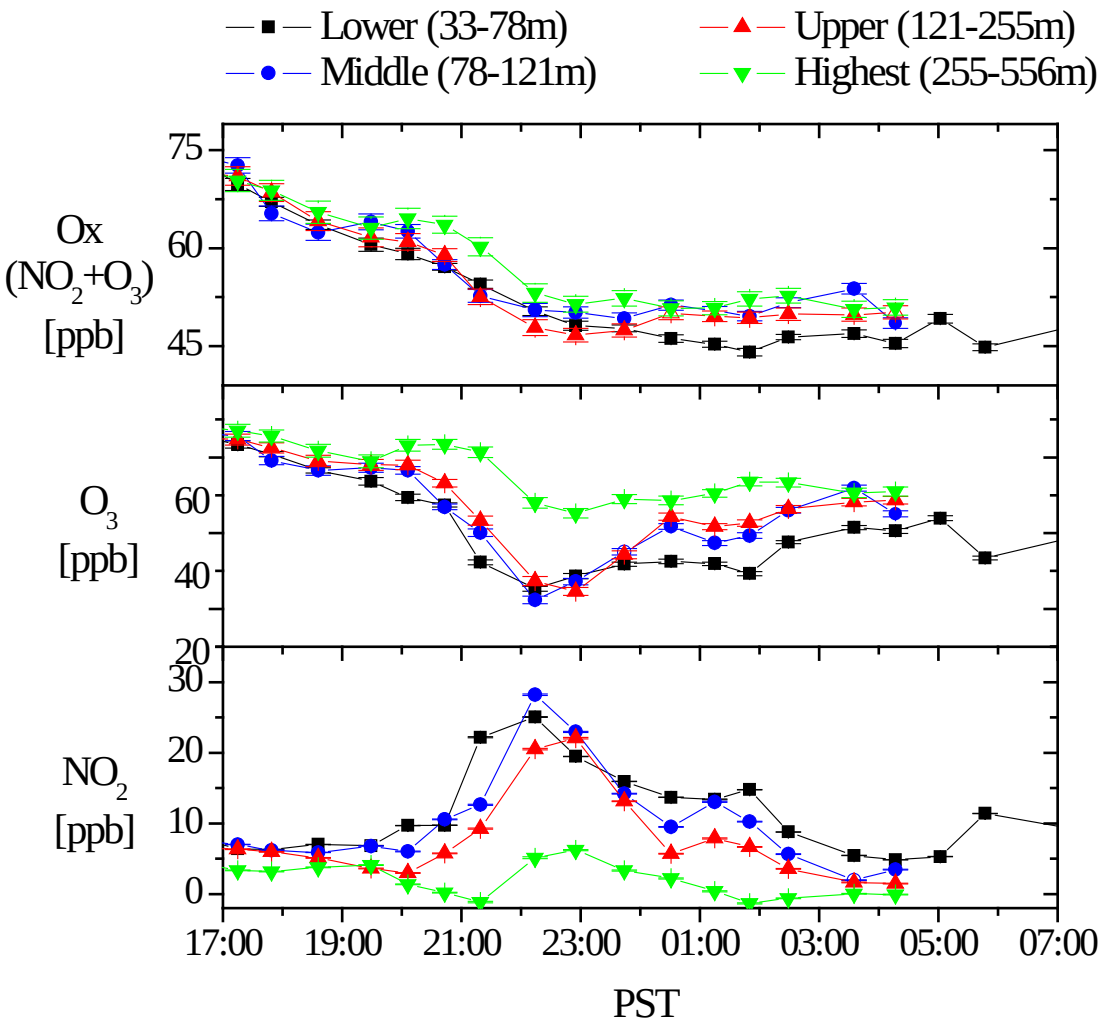

Figure 5.3: O_3, NO_2 and O_x=O_3+NO_2 data during the night of May 29-30, 2010.

This behavior is observed through the entire experiment and shows the impact of nocturnal NO emissions and weak vertical mixing at night. The fact that surface emission and vertical transport of NO together with the simultaneous ongoing titration of ozone by NO: O_3 + NO $\rightarrow$ NO_2 + O_2 is the cause of this behavior and can be shown by plotting the sum of O_3 and NO_2, O_x (Figure 5.3). The very strong gradients in O_3 and NO_2 are not present in O_x, as the titration reaction conserves O_x. It is also interesting to note that O_x slowly decays throughout the night due to the destruction of ozone and NO_2 by NO_3 chemistry, and deposition of O_3 and NO_2 on aerosol and the surface.

HCHO also shows vertical profiles, with higher mixing ratios near the ground during several nights. A possible explanation for the nocturnal vertical profile of HCHO is the impact of direct HCHO emissions by surface HCHO sources. Further analysis of these profiles can be used to determine the HCHO emission rates.

SO_2 typically did not show vertical profiles during the CalNex-LA experiment, indicating that it is not emitted by a surface source at night. However, during a few instances SO_2 plumes that were restricted to the nocturnal boundary layer were observed (Figure 5.4). For example, around 22:00 on 5/24/10 SO_2 mixing ratios in the three lower height intervals increase from around 0.2 ppb to ~0.6 ppb in a short time period. Above 250 m SO_2 does not increase at the same time. This plume of SO_2 is thus constrained to the NBL. It should be noted that the O_3, NO_2, and NO_3 profiles indicate that the highest interval is most likely in the residual layer during this time.

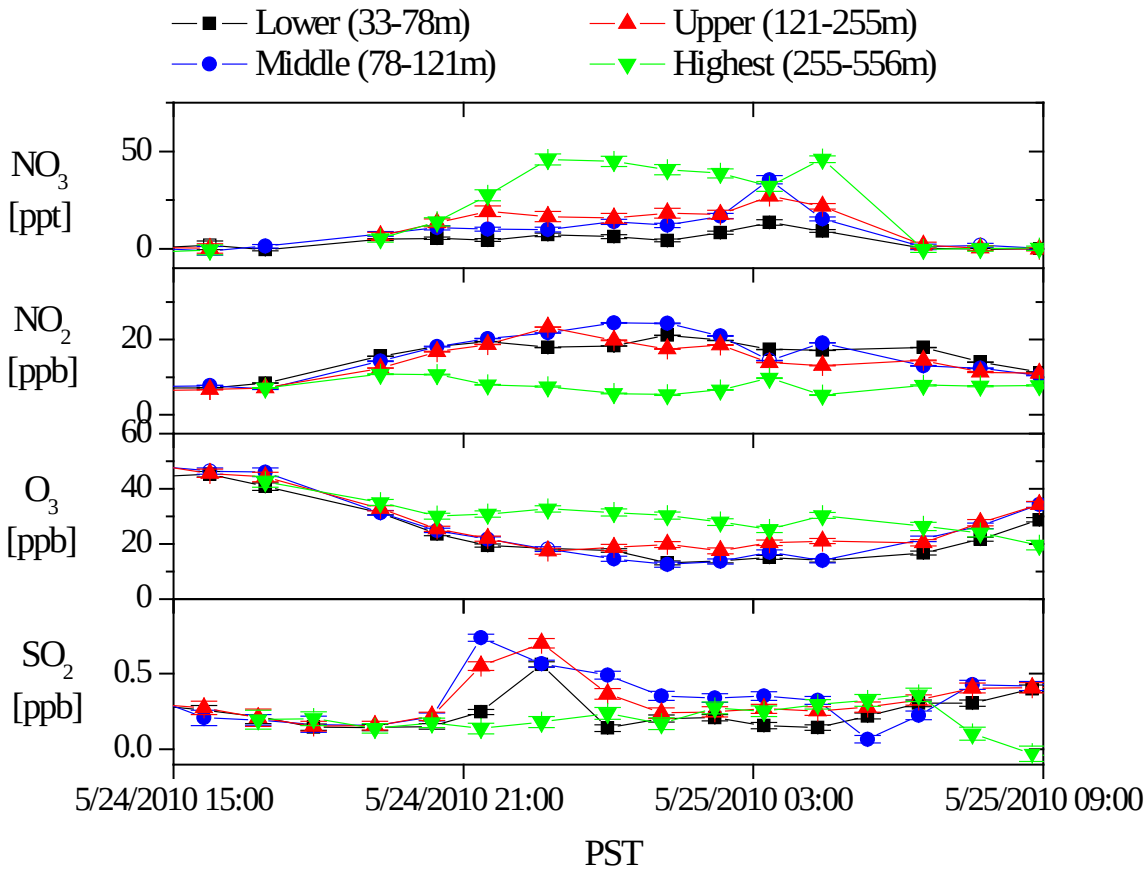

Figure 5.4: Example of a SO_2 plume in the nocturnal boundary layer in the night of May 24-25, 2010.

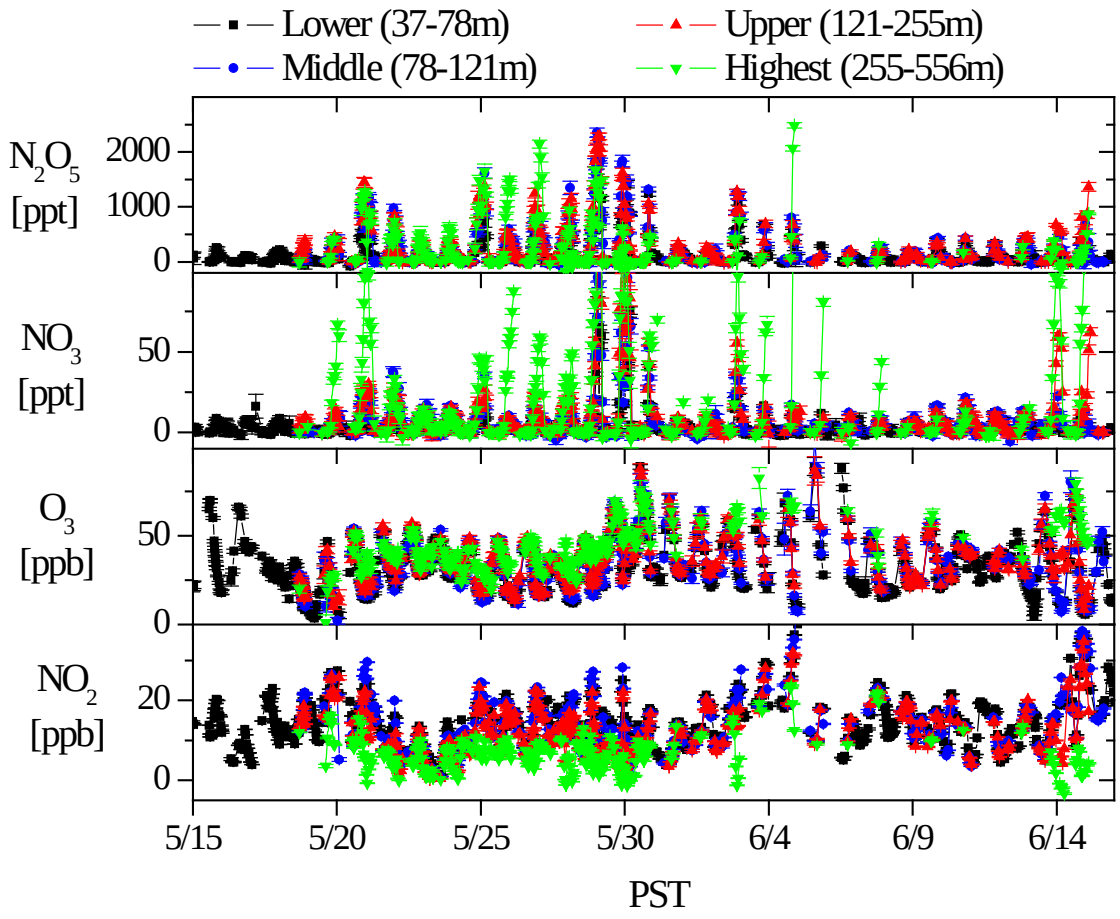

Figure 5.5: Analysis of NO_3 and N_2O_5 chemistry for the night of May 26-27, 2010.

The loss of NO_x at night can proceed through the uptake of N_2O_5 (see Chapter 6). As the LP-DOAS is able to measure the two precursors of N_2O_5, NO_2 and NO_3, and the temperatures are high enough in Los Angeles that the thermal decay of N_2O_5 is relatively fast, we can employ a steady state approach to calculate the N_2O_5 mixing ratio during CalNex-LA (see Figure 2.1 for schematic of NOx chemistry). Using temperature profiles based on interpolation between observations at the surface site and Henninger Flats (location of the highest retroreflector) we calculate the equilibrium constant for the following equilibrium:

$$NO_3 + NO_2 + M \leftrightarrow N_2O_5 + M \qquad K_{eq} = 5.58\text{x}10^{-27} * e^{10724/T} \qquad (5.1)$$

By using the observations of NO_2 and NO_3 in each height interval and the interpolated temperatures, a steady state N_2O_5 mixing ratio was calculated. The uncertainties in NO_3 and NO_2 mixing ratios, as well as that of the temperature were propagated to derive the uncertainties of steady state N_2O_5 mixing ratios.

Figure 5.5 shows an overview of the results of this calculation. N_2O_5 mixing ratios were found to reach above 1 ppb for many nights. It should be noted that the highest N_2O_5 mixing ratios are typically found in the highest height interval. As low clouds often blocked the highest light path, the data in Figure 5.5 appear somewhat skewed. The period from May 20 to May 30, which did not have low clouds, provides a better indication how high N_2O_5 would be in Los Angeles in the absence of low clouds. The N_2O_5 levels are quite high for an urban area with consequences for NO_x and ozone chemistry. We will further discuss NO_3 and N_2O_5 chemistry in the next chapter.

6 NO_3 chemistry and Nocturnal NOx budget

One of the main goals of this project was to study nocturnal NO_3 chemistry and its impact on the NO_x budget. As already discussed above, NO_3 and steady state N_2O_5, are not evenly distributed in the nocturnal boundary layer. As shown in Figure 5.2, NO_3 is highest aloft during many, but not all nights. To further analyze this behavior we first begin with an analysis of the NO_3 steady state lifetime.

6.1 NO_3 Vertical Profiles and Steady State Lifetime

The steady state NO_3 lifetime can be calculated from the measured mixing ratios of NO_2 and O_3 (the NO_3 precursors) and NO_3 itself. As the rate constant is also slightly temperature dependent this was also considered in the calculation shown in Equation (6.1)

$$\tau_{NO3}(PSS) = \frac{k_{NO2+O3}[NO_2][O_3]}{[NO_3]} \qquad k_{NO2+O3} = 1.43x10^{-13} * e^{-2047/T} \tag{6.1}$$

τ_{NO3} is a measure of the chemical activity of NO_3 and can thus aid in the interpretation of its chemistry and the vertical variation of its mixing ratio.

To further analyze NO_3 chemistry we will concentrate on a one week period during CalNex-LA without low clouds and thus full vertical coverage with the LP-DOAS system. This is the same period already discussed in Chapter 5. NO_3 mixing ratios in the lowest 3 height intervals during the beginning of this period were in the range of 20 ppt. On 5/29 and 5/30 NO_3 was much higher and reached up to 150 ppt even near the surface. On other days, the NO_3 mixing ratios in the upper height interval were typically higher and often were at or above 50 ppt during the night. τ_{NO3}, presented in the top panel of Figure 6.1, explains part of this behavior. In the lower three height intervals the NO_3 lifetime was typically in the range of 20–200 seconds. The lifetime in the highest intervals was in the range of 200–1000 seconds during the beginning of this period. The longer lifetime aloft reflects a slower NO_3 chemistry, which is indicative for the highest interval to be in the residual layer. This is confirmed by the Ceilometer aerosol backscatter data (Figure 6.2), which puts the height of the nocturnal boundary layer at 250-300 m during this night. The height of the NBL at the CalNex-LA site was often in this range during the experiment, also explaining the higher NO_3 levels aloft during other nights.

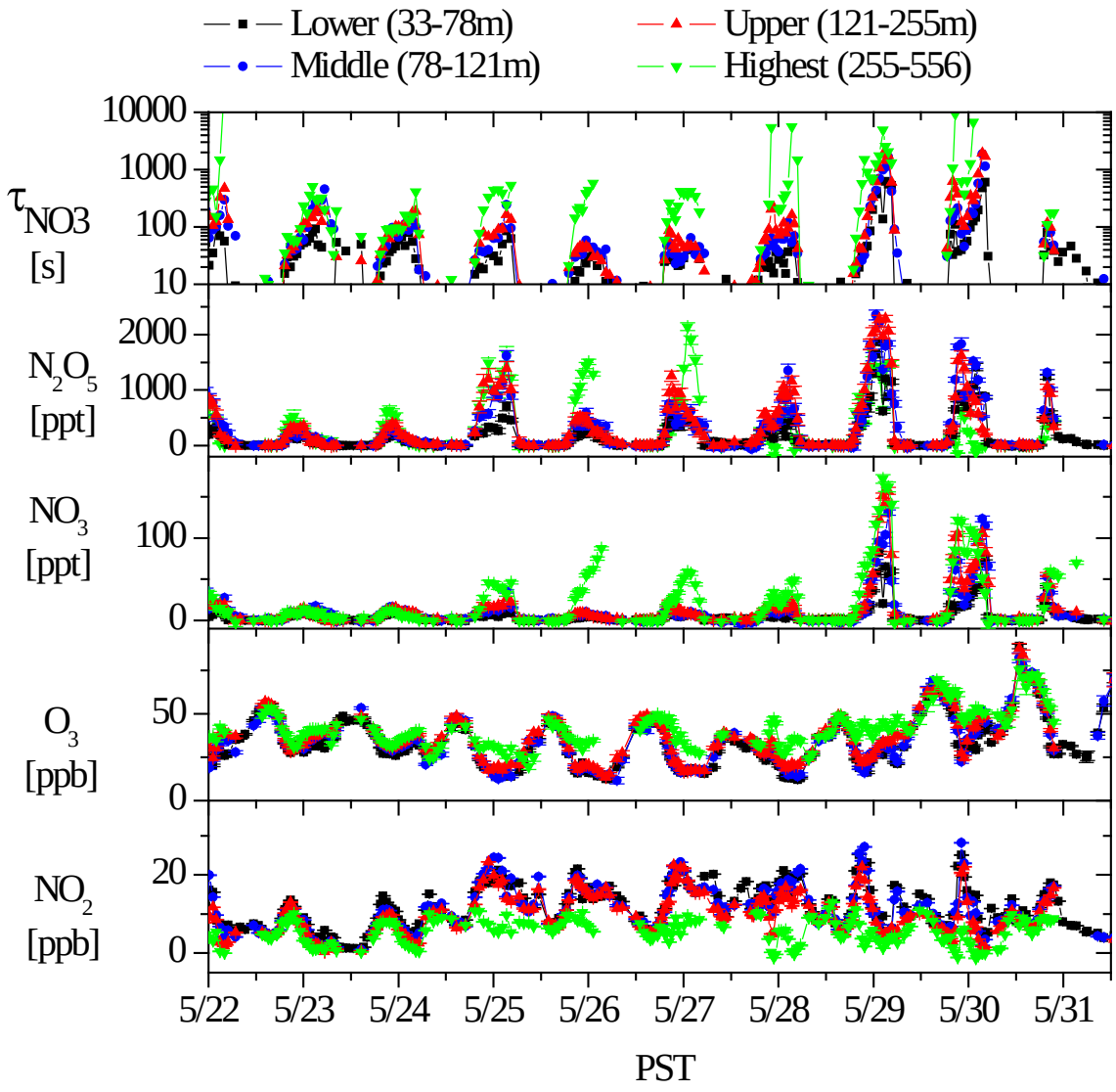

Figure 6.1: Overview of NO_3 chemistry during one week of CalNex-LA

The nights of 5/28-5/29 and 5/29-5/30 (Figure 6.1) are quite unique, as the NO_3 lifetime was elevated throughout all height intervals, with little vertical variation. As a consequence, NO_3 levels were among the highest during the experiment. The lack of a strong gradient in NO_3 and N_2O_5 is quite uncommon. We currently do not have a conclusive explanation for this behavior. The comparison of the in-situ NO_2 and O_3 observations with those from our lowest light path (Figure 3.6) suggest that there was a strong ground inversion that decoupled the surface from aloft. In addition, the nocturnal relative humidity during these nights was the lowest throughout the experiment (Figure 3.4), which could have had an impact on the N_2O_5 uptake coefficient.

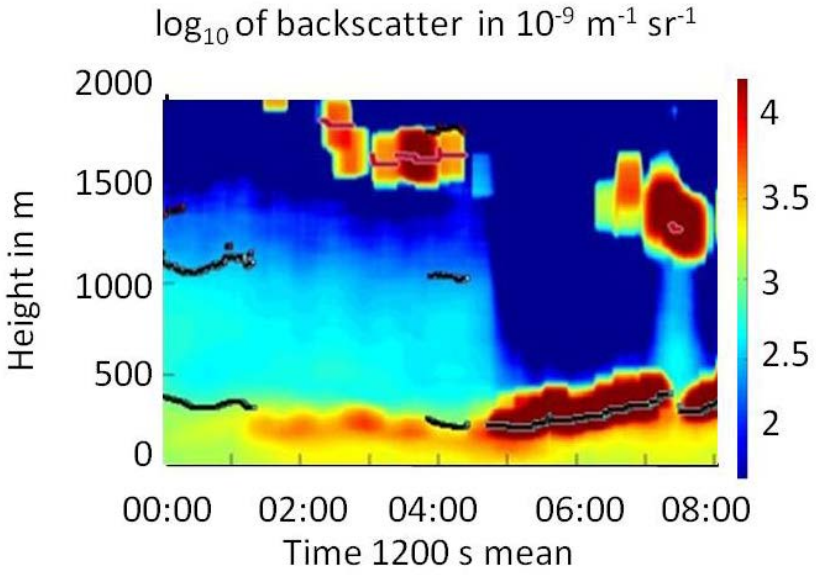

Figure 6.2: Ceilometer observations of aerosol backscatter during the night of May 27-28, 2010. Warm colors indicate higher aerosol levels in the boundary layer.

6.2 Nocturnal NO_x Budget

To determine the nocturnal NO_x budget a detailed analysis of the various NO_3 and N_2O_5 reactions pathways and their vertical dependence is necessary. The following reactions need to be considered in the nocturnal atmosphere:

1. $NO_3 + NO \rightarrow 2\ NO_2$
2. $NO_3 + HC \rightarrow$ organic nitrates $\rightarrow\rightarrow$ SOA
3. $NO_3 \rightarrow$ aerosol
4. $N_2O_5 \rightarrow$ aerosol $\rightarrow NO_3^-$
5. $N_2O_5 \rightarrow$ aerosol $\rightarrow ClNO_2$

Each of these reactions is altitude dependent. An analysis is thus difficult based on field observations alone, in particular when species such as NO, hydrocarbons, and $ClNO_2$, for which vertical profiles were not measured, are involved. Therefore, we used our 1-D Radial Chemistry and Transport model (RCAT 8.2) to gain information on the contribution for these reaction channels.

It should also be noted that the reactions above destroy different numbers of NO_x molecules. Pathway 1, for example destroys no NO_x, while pathways 2 and 3 lead to the loss of one NO_x molecule per reaction. The N_2O_5 uptake (pathway 4) leads to the loss of 2 NO_x molecules.

However, if $ClNO_2$ is produced as a result of this uptake (pathway 5), one NO_x molecule is released back in the morning when $ClNO_2$ is photolyzed.

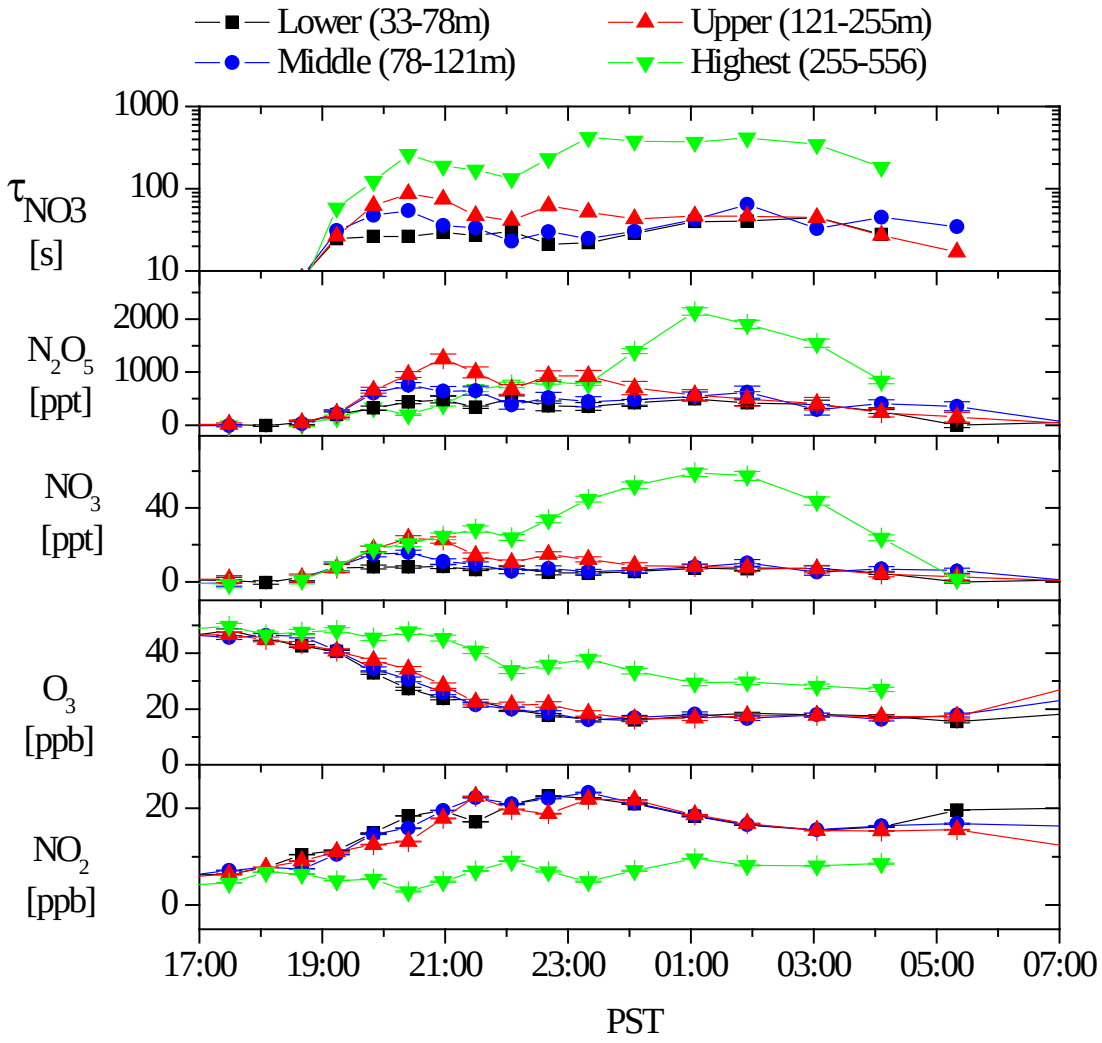

Figure 6.3: Observations of NO_3 and other chemical variables during the night of May 27-28, 2010.

The RCAT model was already described in Section 4.5 and we will restrict the discussion here to the specific model runs for the interpretation of the NO_x loss pathways. We applied the model for one night, May 27 – 28, which is representative of many nights of the CalNex-LA experiment (Figure 6.3). The model was originally initialized with NO emissions rates obtained from a WRF-Chem model run and VOC concentrations measured at Caltech. The WRF-Chem model run was based on the annual emission inventories of Los Angeles County released by the California Air Resources Board in 2005 [http://www.arb.ca.gov/ei/ei.htm] and the initial VOC

concentrations were 1600 ppb of methane, 3.8 ppb of alkanes, 0.09 ppb of biogenic VOC, 1.4 ppb of aromatic VOC, 5 ppb of carbonyls and 0.15 ppb of PANs. The nocturnal atmospheric stability was assumed to be between weakly-stable and very-stable. The values of the stability parameter used (z/L) ranged between 0.8 and 0.2. The vertical profile of aerosol in the model is set to be constant in time, with a aerosol surface area to air volume ratio of 200 $\mu m^2 cm^{-3}$, similar to the observations at the CalNex-LA main surface site. Aerosol and ground uptake coefficients adopted in RCAT 8.2 are $2x10^{-3}$ for NO_3, $2x10^{-5}$ for NO_2, 10^{-4} for HONO, 0.1 for HO_2 and $5x10^{-5}$ for O_3 [*Jacob*, 2000; *Rudich et al*., 1996; *Hu and Abbatt*, 1997; *Michel et al*., 2002].

To improve the model performance we adjusted a number of parameters in the model to better match with the observed vertical profiles of ozone and NO_2. This is necessary as the nocturnal emission rates and vertical stability are often not known well enough to describe the profiles.

Figure 6.4 shows the results of the adaptation of the NO and HC emissions and vertical mixing for that night. While the lower three height intervals are fairly well described in the model, the highest interval shows differences between model and observations. We explain this by the fact that this height interval was in the residual layer, which may have shown different chemical composition than the NBL. Nevertheless the agreement is sufficiently good to allow us to further understand nocturnal NO_3 chemistry. Please note that the purpose of this exercise is not to exactly model the nocturnal atmosphere, but rather to learn more about the systematic behavior of the different chemical processes.

The two other parameters that are not well constrained are the N_2O_5 uptake and the $ClNO_2$ yield. The N_2O_5 uptake coefficient and $ClNO_2$ yield (0.58) were calculated using the formulas shown in *Bertram and Thornton* (2009). The mole fraction of particle liquid water and aqueous phase particle inorganic compounds were calculated each hour using the aerosol chemical composition data measured by CU Boulder as input for the online version of the aerosol inorganic model AIM Model II (http://www.aim.env.uea.ac.uk/aim/aim.php). The calculated N_2O_5 uptake coefficients and $ClNO_2$ yields were averaged throughout the night and input to the RCAT 8.2 model. The result of this calculation was an N_2O_5 uptake coefficient of 0.027. This uptake coefficient lead to a fair description of the observed N_2O_5 mixing ratios during the first half of the night (Figure 6.5). It appears that in the beginning of the night the uptake coefficient is a little too high and further adjustments seem warranted. However, it should be noted that this uptake coefficient is on the higher side of the previously reported values and in agreement with other observations during CalNex from the NOAA WP3 aircraft. During the second half of the night the model under-predicts N_2O_5 compared to the observations. This is most likely due to a change in N_2O_5 uptake, i.e. the uptake coefficient is smaller during the second half of the night. We are currently updating the model to allow for temporal changes in uptake coefficient values, and believe that better agreement between the model and the observations can be achieved this way.

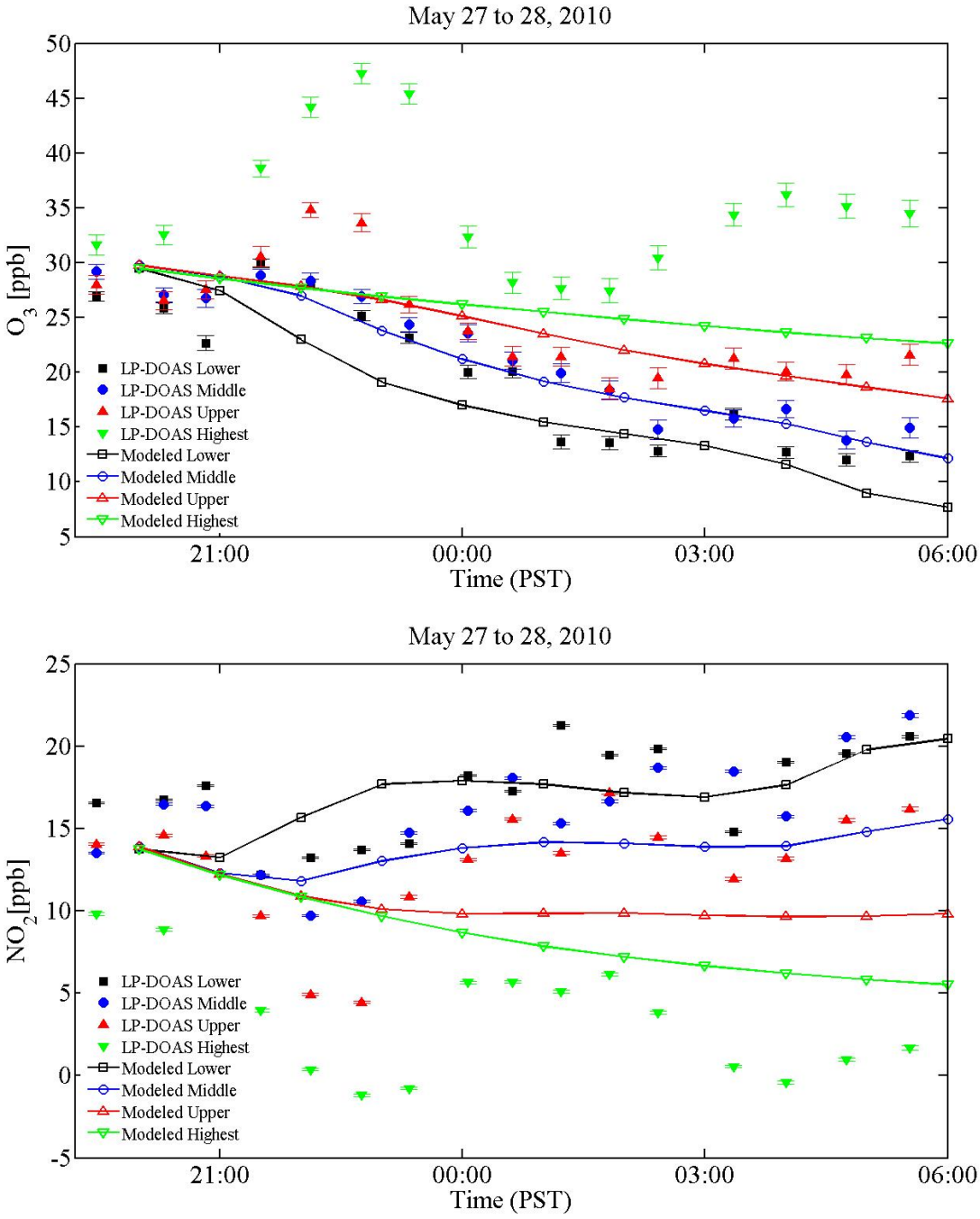

Figure 6.4: Comparison of observations and model output of O_3 and NO_2 mixing ratios in the four height intervals observed by the LP-DOAS.

Using this model run we then compared the observed surface $ClNO_2$ with those from the model at the same altitude, initially using a yield of 0.58 (blue dots in Figure 6.6). Even considering the high variability in the surface $ClNO_2$ data, this yield is too high for this night. We thus lowered the yield in the model to 0.20 (red squares in Figure 6.6) to better describe the amount of $ClNO_2$ in the morning.

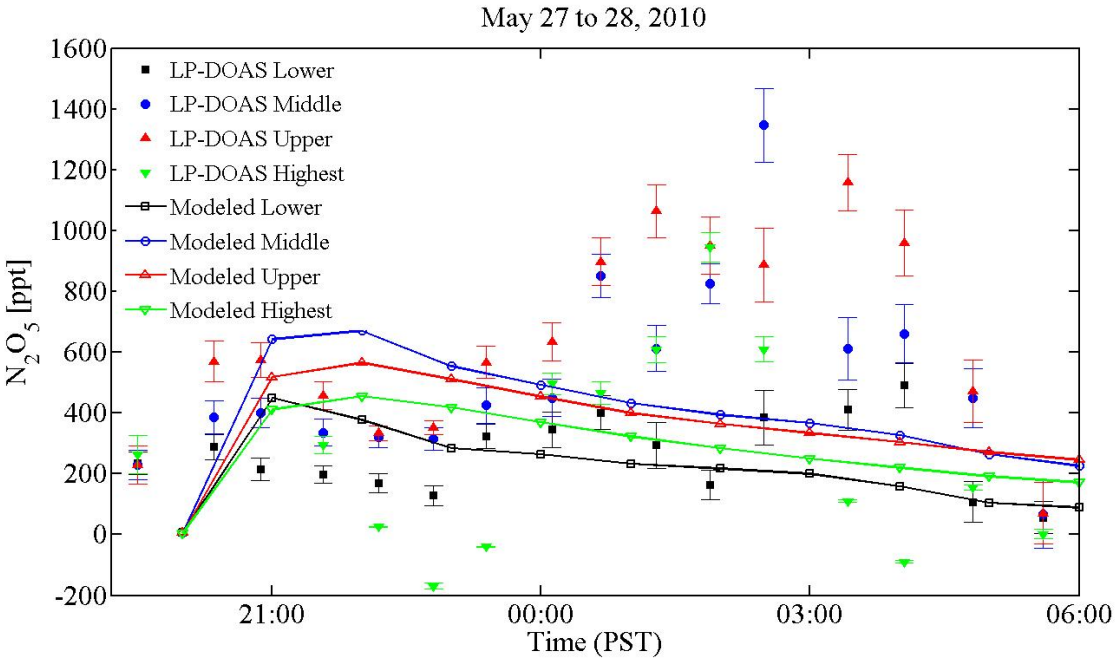

Figure 6.5: Comparison of observations and model output of NO_3 and N_2O_5 mixing ratios in the four height intervals observed by the LP-DOAS.

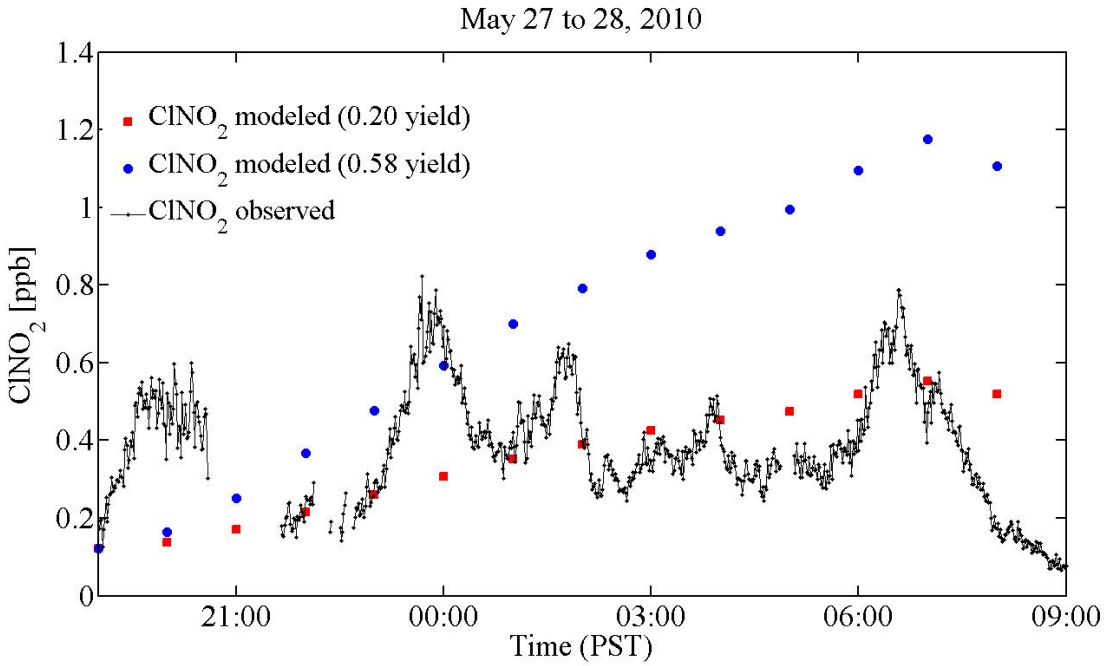

Figure 6.6: Comparison of in-situ observations and model output of surface $ClNO_2$ mixing ratios. The $ClNO_2$ observations were made by L. Mielke and H. Osthoff from the University of Calgary. The figure shows the model calculations for two different yields of the $ClNO_2$ formation.

Based on this model setup we then proceeded to analyze the vertical profiles of NO, α-pinene (as a proxy for terpenes) and $ClNO_2$. Figure 6.7 shows that the modeled mixing ratios of NO decays rapidly with altitude. NO has decayed to negligible values at the height of our lowest height interval at 33 m. The model thus shows that NO has no impact on our NO_x loss calculation, i.e. pathway 1 is unimportant.

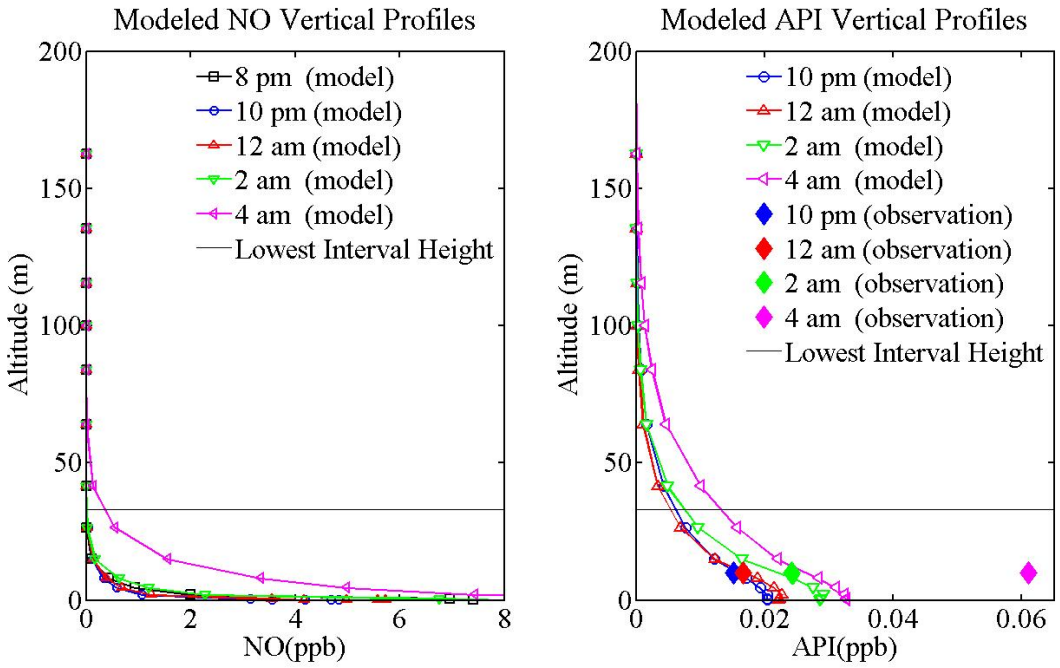

Figure 6.7: Modeled vertical profiles of NO and α-pinene (API) for May 27 and 28. α-pinene observations performed by NOAA are included in the API graph.

The vertical profile α-pinene (Figure 6.7) also decays rapidly with altitude, reducing its impact aloft. To use the surface hydrocarbon observations, for example that of α-pinene also shown in Figure 6.7, to determine the contribution of the NO_3 oxidation, we used the model to determine scaling factors for over 50 hydrocarbons measured by NOAA at the Caltech site. The scaling factors were then used to calculate the loss frequency of NO_3 due to the reaction with hydrocarbons, $f_{NO3}(HC)$, and compared it to the total loss of NO_3 from the pseudo steady state calculation described above, $f_{NO3}(PSS) = 1/\tau_{NO3}(PSS)$, in Figure 6.8. During all nights the loss of NO_3 through its reactions with hydrocarbons is much smaller than the total NO_3 loss. Therefore we can also rule out the reaction of NO_3 with hydrocarbons as a major loss pathway (pathway 2) for NO_x in Los Angeles.

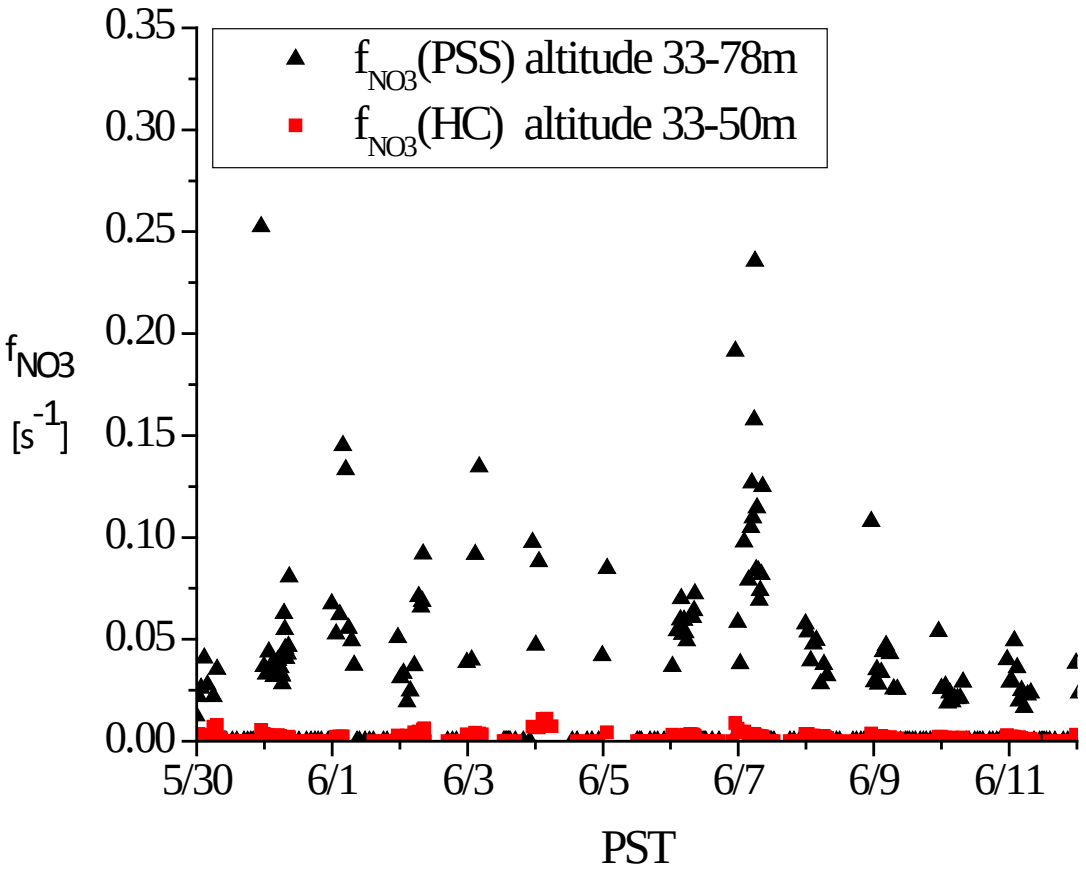

Figure 6.8: Comparison of pseudo steady state loss frequency of NO_3 (black) and the NO_3 loss frequency due to hydrocarbon reactions (red).

An aerosol uptake coefficient of NO_3 ($2x10^{-3}$) as published in the JPL Kinetics review (JPL Publication10-6) was adopted in the 1-D model. This NO_3 uptake coefficient is about an order of magnitude smaller than the uptake coefficient used for N_2O_5. Consequently NO_3 aerosol uptake (Pathway 3) is only a very minor NO_x loss pathway.

Based on the considerations above it is clear that the uptake of N_2O_5 on aerosol is the dominant NO_x loss pathway in Los Angeles. As this pathway will also form $ClNO_2$, which upon photolysis in the morning releases a NO_2 molecule, it is necessary to determine if the $ClNO_2$ surface observations at the CalNex-LA ground site can be used to correct for this effect. We thus expanded our 1-D model to calculate the vertical profile of $ClNO_2$ for the night discussed here (Figure 6.9). While the N_2O_5 vertical profiles in the model showed a strong variation of N_2O_5 mixing ratios, the modeled vertical profile of $ClNO_2$ remained fairly constant with altitude. We explain this by the long lifetime of $ClNO_2$, which allows it to be mixed throughout the NBL. Consequently we can use the $ClNO_2$ surface mixing ratios to determine how much NO_2 is formed from its photolysis in the morning. It should be noted that this result also allows the

determination of the Cl atom formation rate in the morning based on the surface measurements alone.

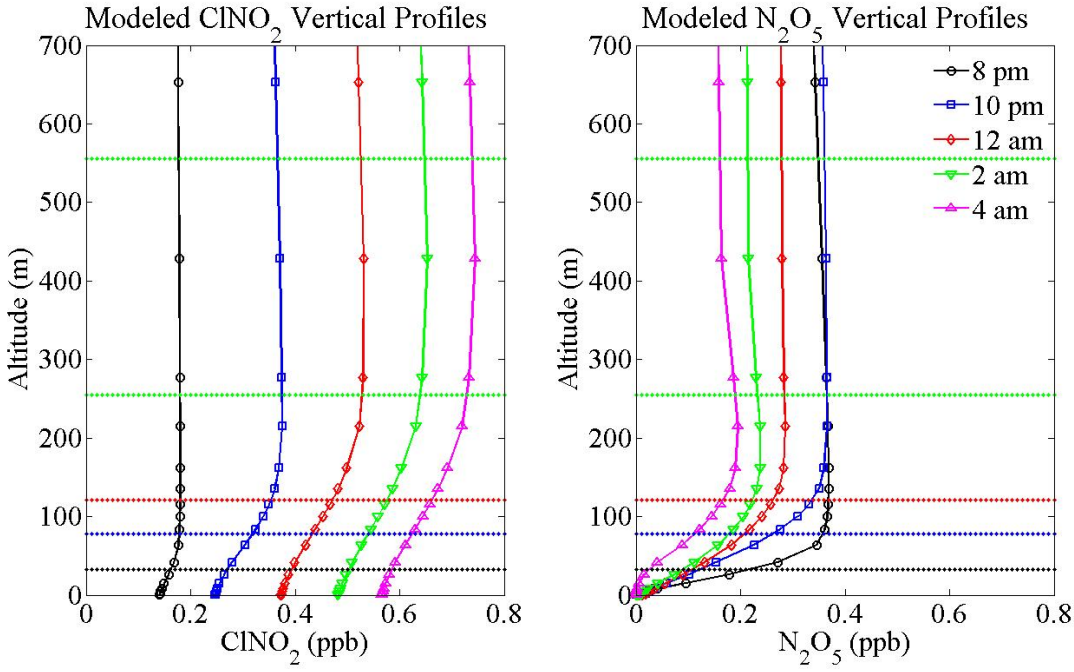

Figure 6.9: Modeled vertical profiles of N_2O_5 and $ClNO_2$ for May 27th to May 28th.

The knowledge that N_2O_5 uptake is the primary NO_x loss process, now allows us to use the NO_3 formation rate $P(NO_3)$ multiplied by a factor of 2, because N_2O_5 uptake destroys two NO_x molecules, minus the $ClNO_2$ morning mixing ratios divided by the length of the night, Δt_{night}, to calculate the NO_x loss rates in the various height intervals (Figure 6.10):

$$LossRate(NO_x)_i = 2 \times P(NO_3)_i - [ClNO_2]_{morning} / \Delta t_{night} \quad (6.2)$$

As expected, NO_x loss rate is highly altitude dependent, with the largest loss near the surface. In addition, the loss varies throughout the night. To eliminate these spatial and temporal dependencies, the loss rates were integrated in altitude (33-556m) and throughout the night to derive a height and time averaged NO_x loss rate. As shown in the cyan bars in Figure 6.10, the loss rate was surprisingly constant, with a range of 0.7 to 1.3 ppb/hr. Similar loss rates were found in Houston in 2006 and 2009, and it appears that this is a typical value that can be used to test if urban airshed models capture the nocturnal NO_x loss correctly.

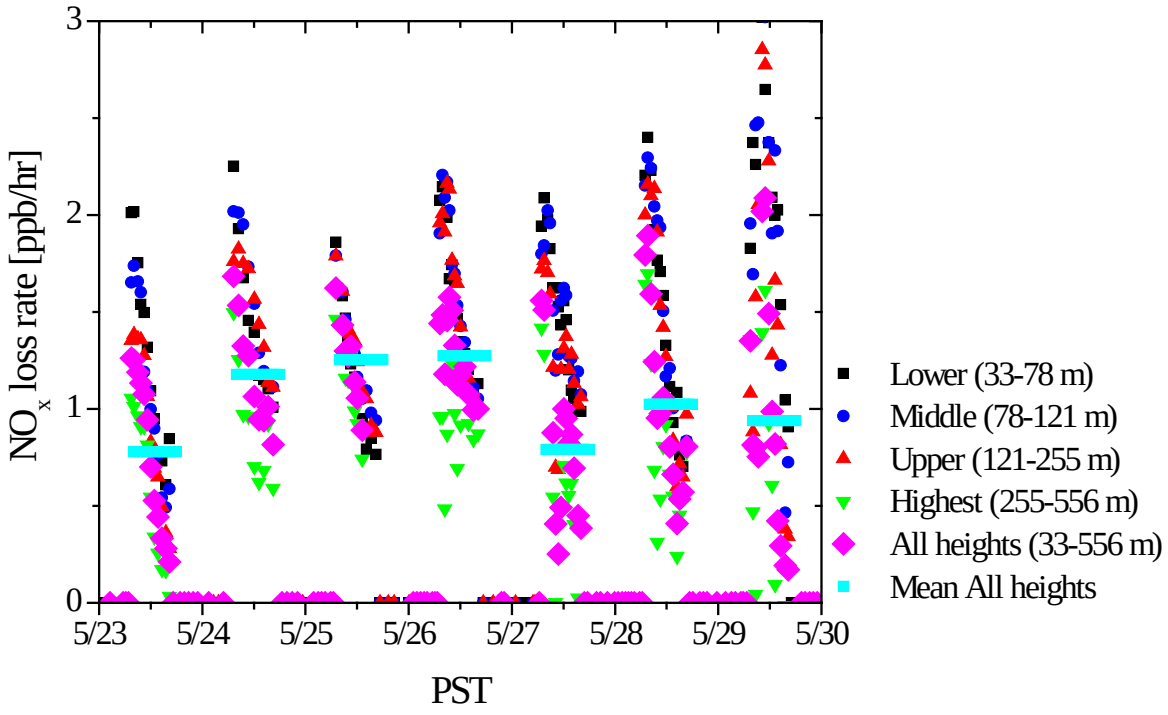

Figure 6.10: Nocturnal NO_x loss during 9 days of the CalNex-LA. The bars in the figure represent altitude and nocturnally averaged loss rates.

6.3 Nocturnal NO_3 Photolysis

Another application of our 1-D model for CalNex was the quantitative analysis of the effect of urban lights on nocturnal chemistry. As reported by Harald Stark et.al. (2011) the downward viewing radiometers on board the NOAA WP3 aircraft observed nocturnal NO_3 photolysis rates over the Los Angeles area originating from urban lights, including street lights, industrial and residential illumination. We collaborated with our NOAA colleagues to use our 1-D chemistry and transport model to provide a better quantification of this effect. We set up and initialized our 1-D model to approximately reproduce the vertical trace gas profiles observed by the WP3. Our base case scenario (Figure 6.11) does not include urban light NO_3 photolysis. Two sensitivity runs with $J_{NO3} = 10^{-5}\ s^{-1}$ and $J_{NO3} = 5\times 10^{-5}\ s^{-1}$, respectively, were performed (Figure 6.11).

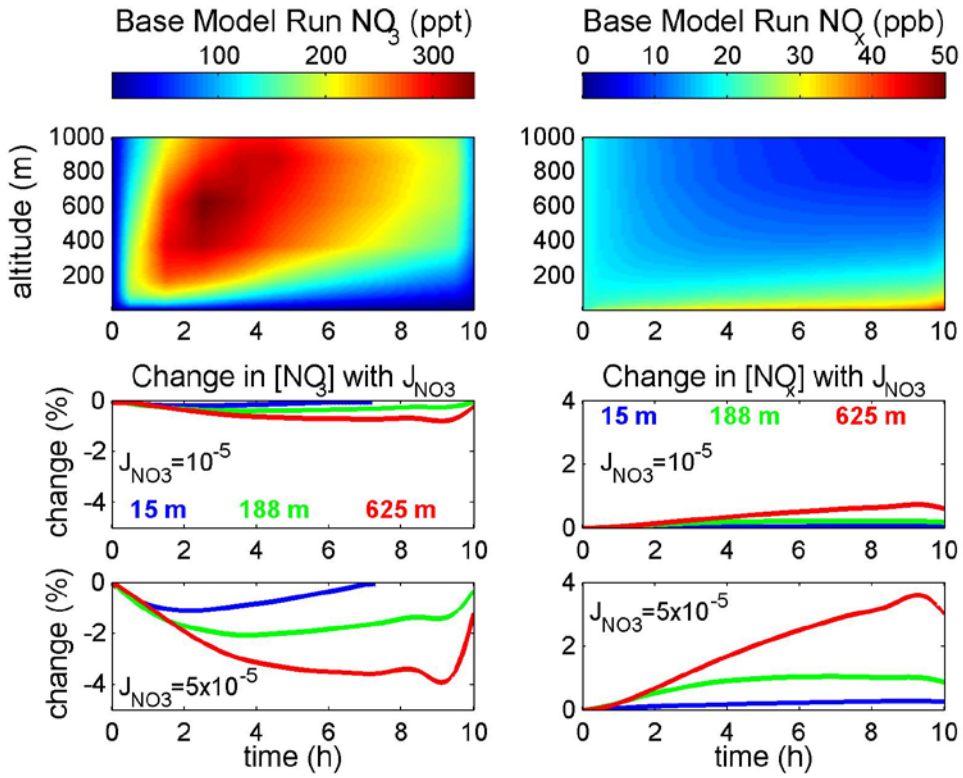

Figure 6.11: 1-D model runs to quantify the impact of nocturnal NO_3 photolysis from urban light sources. The top two panels show the base case results for NO_3 and NO_x. The lower panels show the impact of nocturnal NO_3 photolysis on NO_3 and NO_x mixing ratios at three altitudes.

The top panels in Figure 6.11 show the NO_3 and NO_x vertical profiles throughout one night for the base case. The profiles follow the general behavior of larger NO_3 mixing ratios aloft and larger NO_x near the surface. The bottom panels in Figure 6.11 show the relative change in NO_3 and NO_x mixing ratios at three altitudes (15 m, 188 m, 625 m) in the model domain for the two NO_3 photolysis frequencies. The impact of $J_{NO3} = 10^{-5}$ s^{-1} is quite small. The impact of $J_{NO3} = 5\times 10^{-5}$ s^{-1}, which is on the high end of the observed J_{NO3} values, at 625 m altitude is in the range of -4% for NO_3 and +4% for NO_x. As shown in Figure 6.11 NO_3 chemistry occurs predominately between 100-200 m and 1000 m altitude, the change in the NO_3 and NO_x budget at 625 m describes a large part of the atmosphere that will become the daytime boundary layer during the next day. As 625m altitude shows some of the highest NO_3, the effect of photolysis is slightly higher at this altitude than the boundary layer average.

The results show that nocturnal photolysis of NO_3 from anthropogenic light sources can decrease NO_3 levels at night. This, on the other hand, leads to a lower nocturnal NO_x loss and consequently more NO_x in the morning, which is then available for ozone formation. Another consequence from the nocturnal photolysis is slightly higher ozone levels in the early morning, as elevated NO_x, which at night aloft is predominately NO_2, photolyzes during sunrise. Nevertheless, the effect is likely rather small for the entire Los Angeles Basin. The results of this study have been published in Nature Geosciences [*Stark et al.*, 2011].

7 HONO Chemistry

Another focus of our study was the investigation of nitrous acid (HONO) chemistry and its impact on the OH budget during the morning, and, considering recent findings on the presence of daytime HONO, also during the day.

7.1 HONO Observations

Our analysis is based on the LP-DOAS measurements already briefly described in Chapter 5. In addition, we use data from two in-situ instruments deployed at the Caltech ground-site:

Incoherent Broadband Cavity Enhanced Absorption Spectrometer (IBBCEAS): This instrument, which was developed and deployed by C. Young, R. Washenfelder, and S. Brown from NOAA-ESRL, is based on a very similar approach to the DOAS instrument, except that the long absorption path-length is folded in a multireflection cell into a small volume. The instrument samples air through an inlet and thus measures the in-situ HONO concentrations. The IBBCEAS cell was deployed on the gas-sampling tower at an altitude of 10m above the ground. Details of the IBBCEAS instrument can be found in *Washenfelder et al*. (2008).

Chemical Ionization Mass Spectrometer (CIMS): The Acid-CIMS instrument was developed and deployed by P. Veres, J. deGouw and J. Roberts from NOAA-ESRL during the CalNex LA-experiment. In short, the instrument is based on the soft ionization of trace gases via proton transfer from the CH_3COO^- ion. It measures a range of acids, including HONO, at a high time resolution. Here we will report 10 min averages of this system. The Acid-CIMS was deployed at 3 m altitude above the ground during the CalNex-LA experiment. Details of the instrument can be found in *Veres et al.* (2008).

While it is common to intercompare different systems measuring the same trace gas during field experiments, it will become clear in the following analysis of the data that this is not possible, or at least extremely difficult for the very altitude dependent HONO measurements.

For our analysis we will also use observations from a number of other instruments deployed at the CalNex LA site. A chemiluminescence with photolytic converter NO_2 system was used by the University of Houston to measure NO_2 at 10m altitude by photolytically converting it to NO and then measuring NO by the well-known chemiluminescence approach (J. Flynn and B. Lefer from the University of Houston). The same group also measured actinic fluxes and photolysis rates using a Scanning Actinic Flux Spectroradiometer [*Shetter and Muller*, 1999].

7.2 Results

Figure 7.1 shows a three day example of the HONO observations from the three different instruments. The maximum levels measured near the surface approached 3 ppb during the night of 6/13 – 6/14. It is also obvious that the measurements show an altitude dependence at night, and also during the day, which makes the interpretation of line plots such as in Figure 7.1 difficult, in particular when providing a long-time overview of the observations.

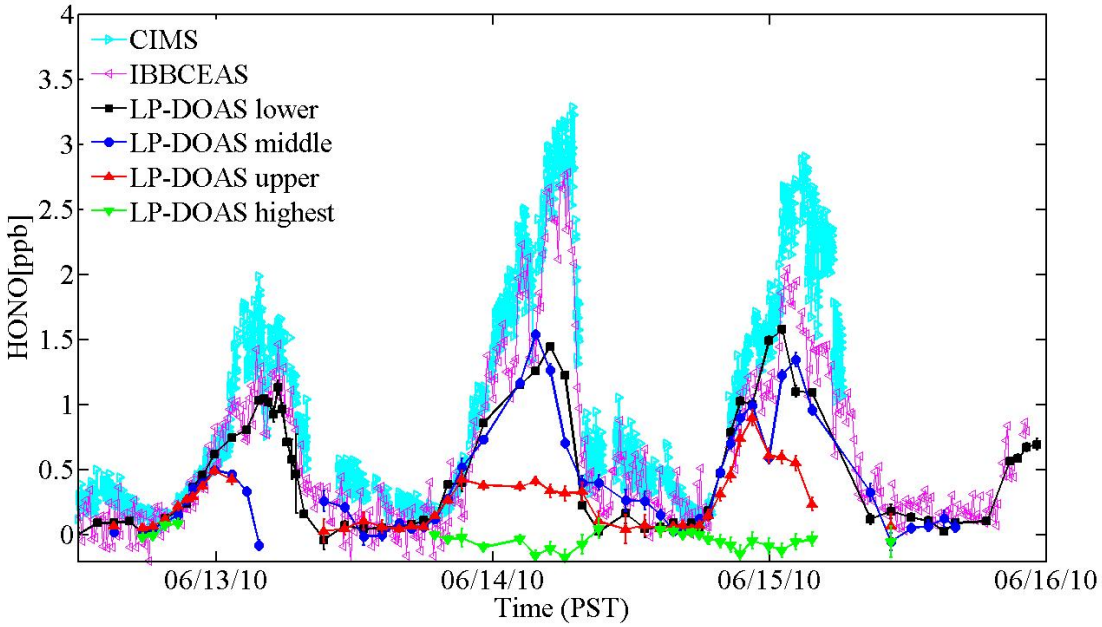

Figure 7.1 Overview of three days of simultaneous observations by the two in-situ HONO instruments and the HONO levels in the four LP-DOAS height intervals.

We thus used the NO_2 and HONO data to make profile color plots (Figures 7.2 and 7.3). It should be noted that these plots are based on a linear interpolation between the different measurements and should thus only be considered a visualization of the data, rather than the exact data itself. The white areas in Figure 7.2 and 7.3 indicate missing DOAS data aloft due to the presence of low clouds blocking the upper light paths.

The visualized NO_2 and HONO mixing ratios (Figure 7.2 and 7.3) show high mixing ratios of both species during every night near the surface. NO_2 mixing ratios are often enhanced up to the top of the NBL, which is indicated by the black line in the figures. The agreement of the NO_2 profile and the NBL height is not perfect due to the difficulty of determining the BL height from the LIDAR at night and the poor spatial resolution and the interpolation from the DOAS data above 200 meters altitude. Nevertheless, a qualitative relation can be seen. This behavior of NO_2 is caused by emissions of NO_x near the surface that are trapped in the NBL.

The enhanced HONO mixing ratios are typically located lower in the atmosphere than the NO_2 cloud. The profiles often decrease sharply above 50 m. Only during a few days were substantial HONO mixing ratios observed above 100 m agl. Noteworthy are the nights of 6/14 and 6/15 when HONO remained above 1 ppb up to 200 m agl. This is rather unusual behavior for this species and the cause and impact of these large HONO levels needs further investigation.

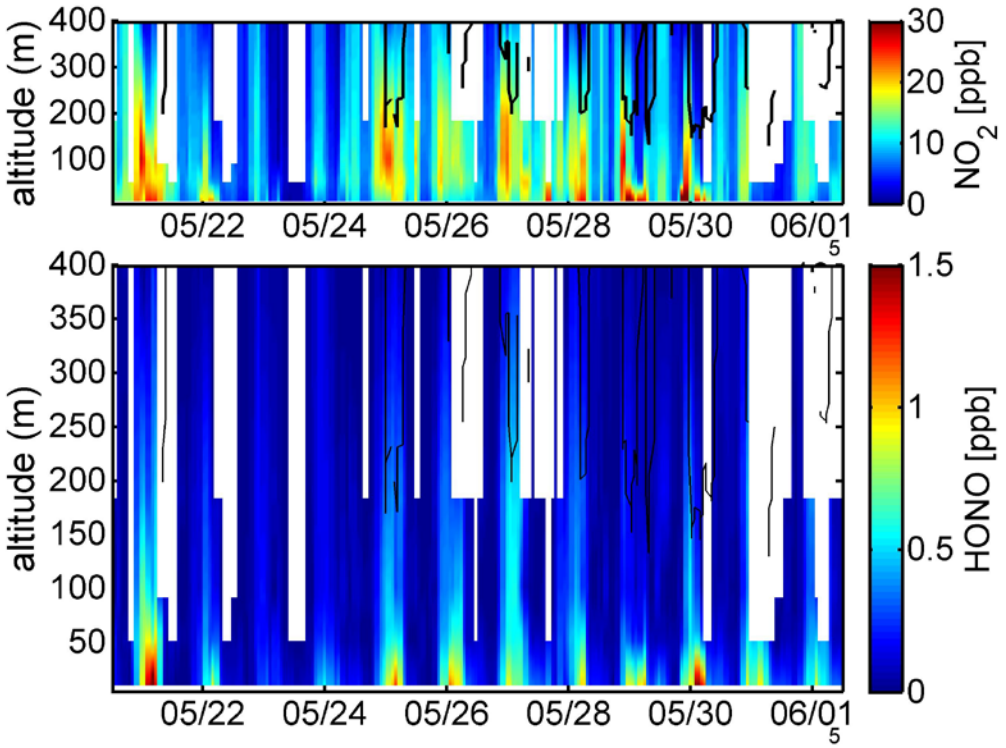

Figure 7.2 Overview of the NO_2 and HONO vertical distribution from May 20 to June 2, 2010. The black line in the figure shows the boundary layer height retrieved from a Ceilometer. White areas in the figure indicate missing data from the upper LP-DOAS paths due to low clouds.

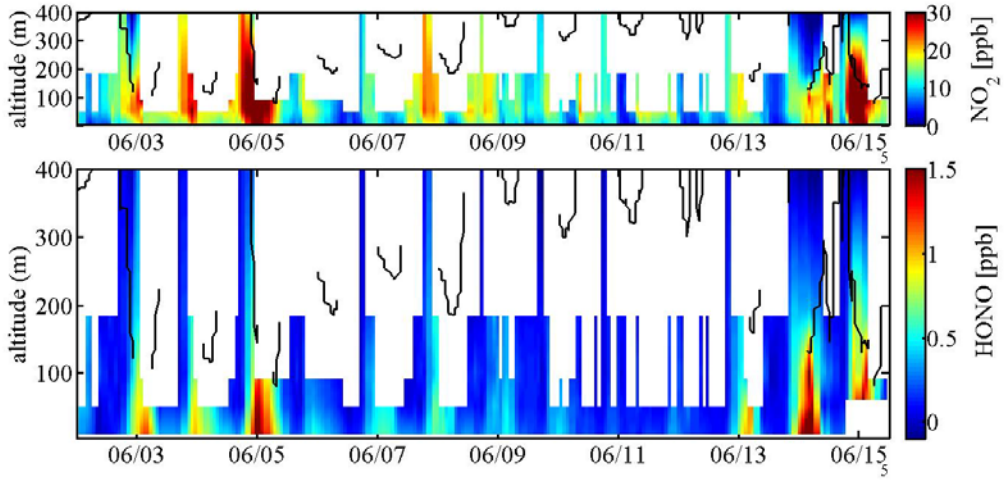

Figure 7.3 Overview of the NO_2 and HONO vertical distribution from June 2 to June 16, 2010. The black line in the figure shows the boundary layer height retrieved from a Ceilometer. White areas in the figure indicate missing data from the upper LP-DOAS paths due to low clouds.

7.3 Nocturnal HONO Formation

An overview of the HONO data during the last three weeks of the CalNex experiment (Figures 7.2 and 7.3) shows that surface mixing ratios above 1 ppb are common in Los Angeles. However, the HONO mixing ratios decrease substantially with altitude, which poses a challenge for the understanding of HONO formation and the impact of HONO photolysis.

To study the formation of HONO we have extracted vertical profiles for one night of the experiment, May 27-28, 2010. The choice of this night was mostly due to our analysis of NO_3 chemistry, which was also performed during this night. We will analyze more nights in the future. The vertical HONO profiles throughout the night (Figure 7.4) show a steady increase of HONO mixing ratios near the surface and a much slower increase aloft. At the surface HONO reaches ~1.2 ppb, while the levels above 200 m agl are typically below 0.25 ppb.

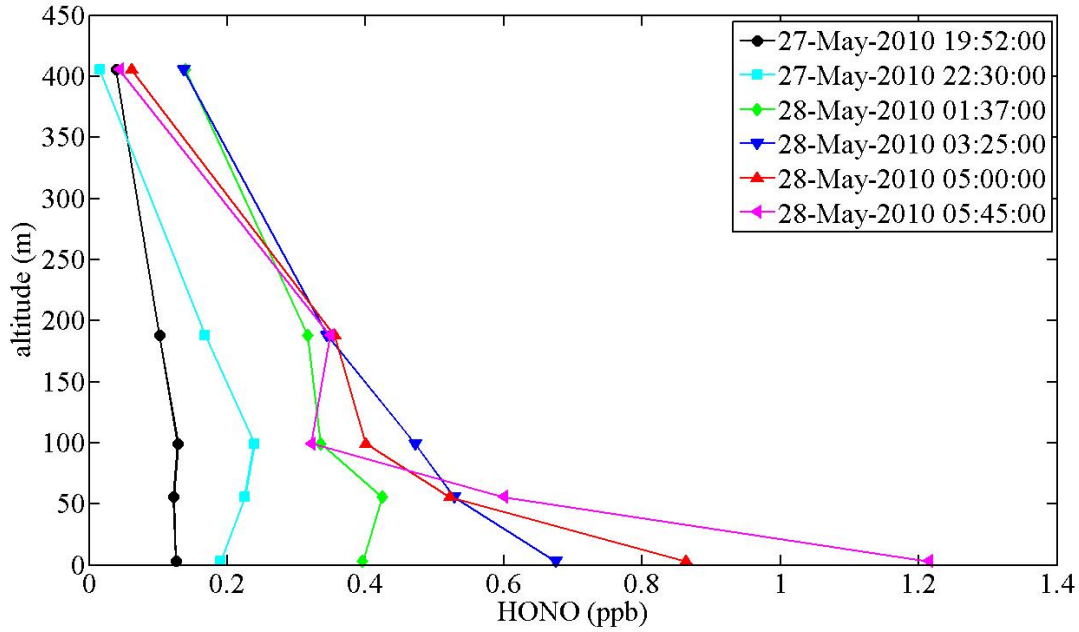

Figure 7.4: Vertical profiles of HONO mixing ratios for the night of May 27-28, 2010.

To further understand the mechanisms that lead to the observed HONO profiles we have used the model described in Section 4.5. The model is unique, as it has logarithmic grid spacing below 1 m height. Surface reactions are calculated explicitly through a calculation of the molecular collisions with the surface and reactive uptake coefficient, i.e. the probability of a reaction. In addition, the model also calculates the heterogeneous reactions on the aerosol

Figure 7.5 illustrates the HONO formation parameterization in the model, which has been previously employed to study HONO profiles in Houston, TX [*Wong et al.*, 2011a]. The only difference from our previous parameterization is the slightly higher uptake coefficient for the NO_2 to HONO conversion of $\gamma = 2\times 10^{-5}$. For the Houston study $\gamma = 10^{-5}$ was used, which was derived from laboratory measurements of aged asphalt [*Trick.*, 2004]. The NO_2 conversion had a

50% yield according to the $NO_2 + NO_2 + H_2O \rightarrow HONO + HNO_3$ reaction that has been found to be first order in NO_2. The surface loss of HONO, which was also determined in the laboratory, was $\gamma = 10^{-4}$. A constant aerosol surface to air volume ratio of S = 200 $\mu m^2 cm^{-3}$ with same uptake coefficients was used to describe aerosol chemistry. The model also considers direct emissions of HONO, which are linked to those of NO_x with an emission ratio of $HONO/NO_x$ = 0.008 [*Kurtenbach et al*, 2001].

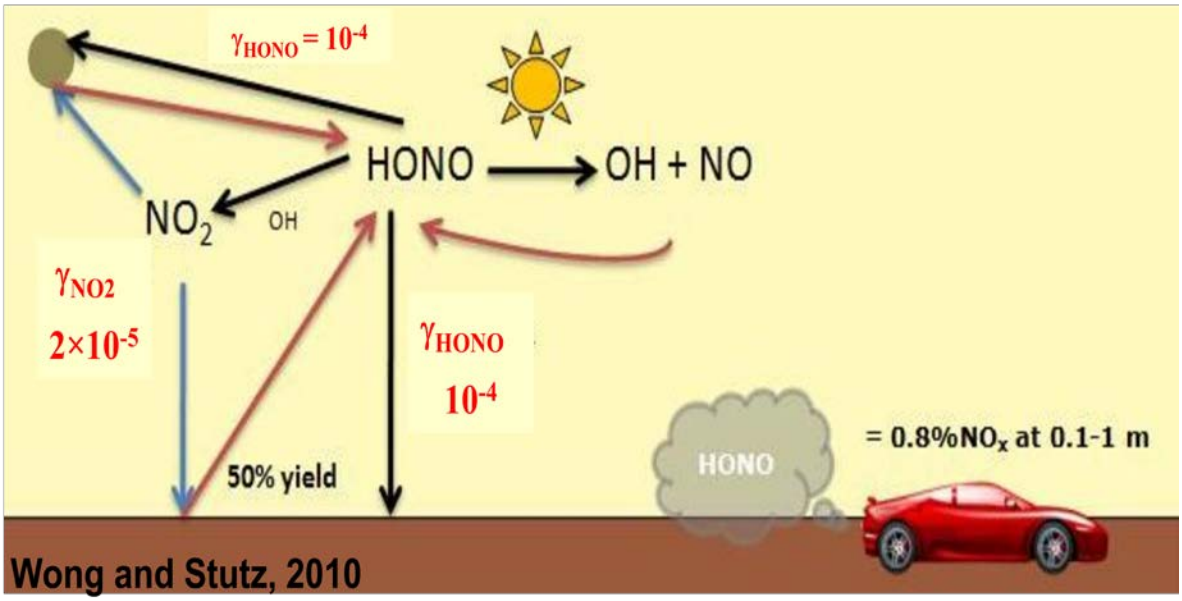

Figure 7.5: Parameterization of HONO surface chemistry used in the 1-D chemistry and transport model (from *Wong et al.* (2011a)).

This parameterization was included in the model runs used to study nocturnal NO_3 chemistry (see Section 6.2). It should be noted that only the vertical mixing and the emission rates were adjusted to make the model simulate O_3 and NO_2 vertical profiles similar to those observed. No attempt to tweak the model to correctly simulate HONO was made.

The modeled HONO profiles (Figure 7.6) show a behavior very similar to the observations, except for the lowest part of the atmosphere in the first few hours of the night. In general, the model predicts a steady increase of HONO mixing ratios through the night to up to 1 ppb near the surface, and a much slower increase aloft. The maximum modeled HONO mixing ratio aloft is ~0.2 ppb. The model also captures the shape of the profile, which, considering the limitations of the observations, agrees fairly well. The differences in the shape near the surface are most likely due to local effects, such as shear induced mixing, in the observations.

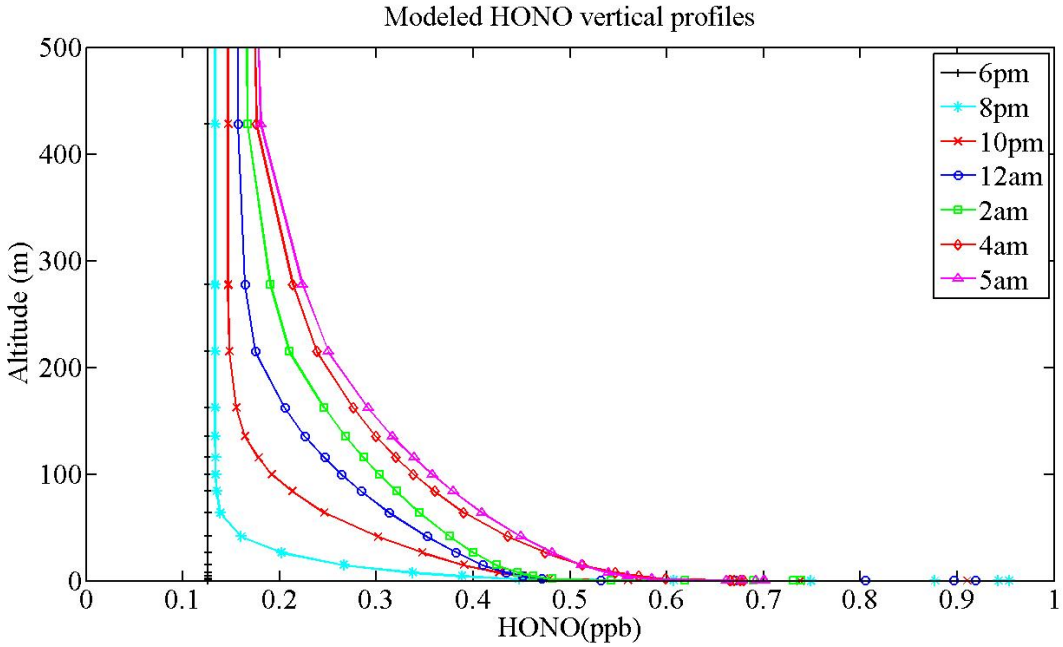

Figure 7.6: Modeled HONO vertical mixing ratio profiles for May 27-28, 2010.

The conclusion that can be drawn from this exercise is that HONO is predominately formed through NO_2 conversion at the surface. It is comforting that the same parameterization, with only a slight difference in the NO_2 to HONO reactive uptake coefficient, was successful in Houston and Los Angeles [*Wong et al.*, 2011a]. It thus appears that the formation of HONO can be explained by a relatively simple chemical mechanism, as long as vertical mixing and emissions are correctly represented in a model. Our analysis indicates the dominance of the conversion of NO_2 to HONO on the surface. Our model indicates that the aerosol mediated NO_2 to HONO conversion and that direct HONO emissions only play a minor role. While we have thus far only analyzed one night during CalNex in detail, we plan to focus on a few more nights to confirm these findings.

7.4 Daytime HONO

An interesting and very important aspect of HONO chemistry is the question of its daytime mixing ratios and how HONO is formed during the day. To answer the first question we calculated the hourly averaged HONO mixing ratios from the two in-situ instruments and all four LP-DOAS height intervals throughout the CalNex experiment (Figure 7.7). These values are compared to a steady state HONO mixing ratio expected if one assumes that the only chemical reaction forming HONO during the day is OH + NO:

$$HONO_{SS} = \frac{k\,[OH][NO]}{J_{HONO}} \tag{7.1}$$

$HONO_{ss}$ was calculated from the direct observations of OH radicals by the University of Indiana and observations of NO and the HONO photolysis rate, J_{HONO}, made by the University of

Houston. These measurements were all made at 10 m altitude at the CalNex-LA ground site; $HONO_{SS}$ thus represents a 10 m value.

The formation of HONO through the OH + NO reaction is represented in Figure 7.7 by the $HONO_{ss}$ line. $HONO_{ss}$ was calculated from the observations of OH, NO, and J_{HONO} using the pseudo-steady-state between the OH + NO $\rightarrow$ HONO formation reaction and HONO photolysis. $HONO_{ss}$ is considerably smaller than the observations in the lowest 250m of the atmosphere, clearly indicating the existence of an additional HONO source. Only above 250m agl are the $HONO_{ss}$ values comparable to the observations. However, we do not have OH and NO observations above 250m and further modeling analysis is needed to confirm if the OH + NO reaction is the only source of HONO aloft

It is obvious from Figure 7.7 that the different hourly averaged HONO datasets do not agree with each other. All observations, except perhaps the HONO measured in the highest interval, are higher than $HONO_{SS}$, showing that another daytime HONO source would be active. This daytime source is a direct OH radical source that is currently not considered in most air quality models. We will discuss this source further in Section 7.5.

The in-situ instruments report considerably higher HONO mixing ratios than does the LP-DOAS. This discrepancy has been observed at various other locations and has been a topic of debate for several decades, i.e. most comparisons show lower data from the open air LP-DOAS observations compared to other methods.

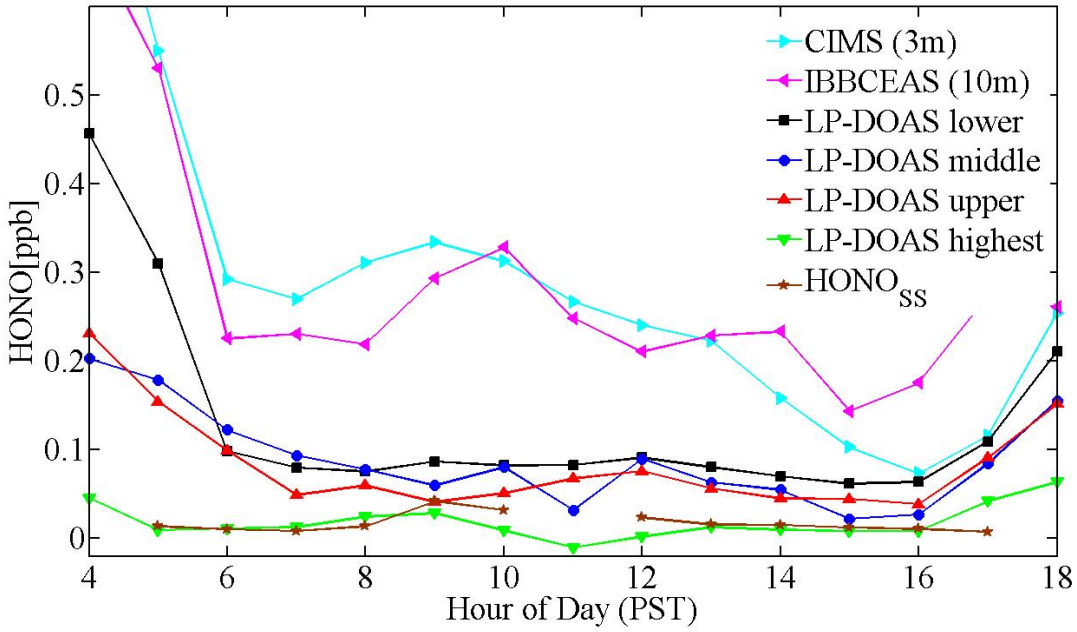

Figure 7.7: Hourly averaged HONO mixing ratios (PST) from the two in-situ instruments and the four LP-DOAS height intervals throughout the CalNex-LA experiment. Also shown is steady state HONO, $HONO_{SS}$, calculated through the OH + NO reaction and HONO photolysis averaged throughout the CalNex-LA Experiment.

While it appears that the different instruments do not agree, a different look at the data (Figure 7.8) shows that the difference between the in-situ and path-averaged measurements is most likely not caused by instrumental problems but rather by strong vertical profiles of HONO during the day. While the in-situ instruments in the lowest 10 m of the atmosphere show mixing ratios between 200 and 300 ppt, the LP-DOAS indicates mixing ratios in the range of ~70 ppt at 50 m altitude and 20 ppt at 400 m altitude. This behavior is at first rather surprising, as the daytime boundary layer is often assumed to be well mixed, and the HONO lifetime against photolysis is in the range of 15 minutes.

To better analyze the daytime HONO data we plotted vertical profiles at three hours throughout the day in Figure 7.8. A clear and relatively smooth vertical profile can be seen. While we have not yet run our 1-D model to simulate the daytime HONO profile in Los Angeles, HONO profiles calculated for Houston, TX, look very similar to those in Figure 7.8.

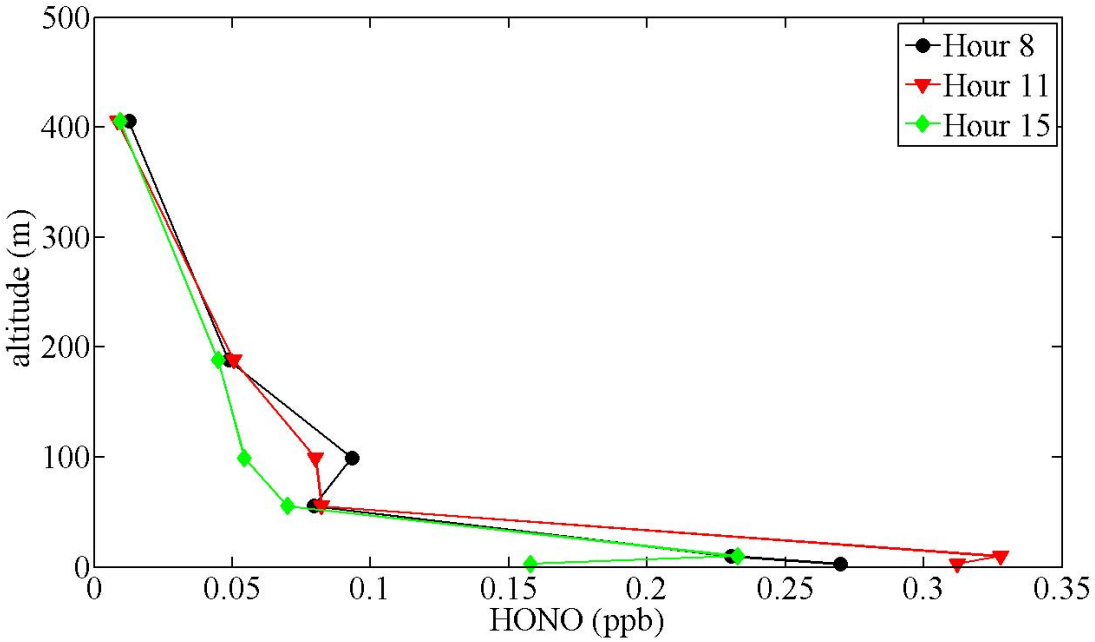

Figure 7.8: Observed hourly averaged HONO mixing ratio profiles for 9:00, 12:00, and 16:00.

Similar to nighttime, observed HONO levels near the surface are considerably larger than aloft during the day. This is indicative of a surface reaction, rather than a volume reaction due to gas-phase or aerosol chemistry. To further analyze the source of HONO, one can consider various possible formation pathways, following the approach of *Wong et al.* (2011b). We can distinguish three different pathways to form HONO in the daytime atmosphere:

1) A gas-phase source, such as the proposed formation of excited NO_2, NO_2^*, with water vapor [*Li et al.*, 2008].

2) An aerosol source, such as the photolysis of particulate nitrate or the photo-enhanced conversion of NO_2 on the aerosol surface [*Stemmler et al.*, 2007].

3) A photochemistry-enhanced surface conversion of NO_2 [*Kleffmann*, 2007].

Following the argument by *Wong et al.* (2001b), we calculated the diurnal profile of the $HONO/NO_2$ ratio for all six altitudes (Figure 7.9). The surface HONO observations exhibit a diurnal profile of $HONO/NO_2$, that can be explained by a photolytic surface source of HONO. The vertical profile of HONO as well as the lower $HONO/NO_2$ ratios aloft can be explained by the photolysis of HONO as it is mixed upwards in the atmosphere. The comparison of $HONO_{SS}$ with HONO in the highest interval seems to suggest that there is only a minor contribution of a gas-phase or aerosol source of HONO in Los Angeles. The detailed analysis of the daytime HONO observations is beyond the scope of this nighttime chemistry project. Nevertheless, we will perform these calculations in the near future and will share our results with the ARB.

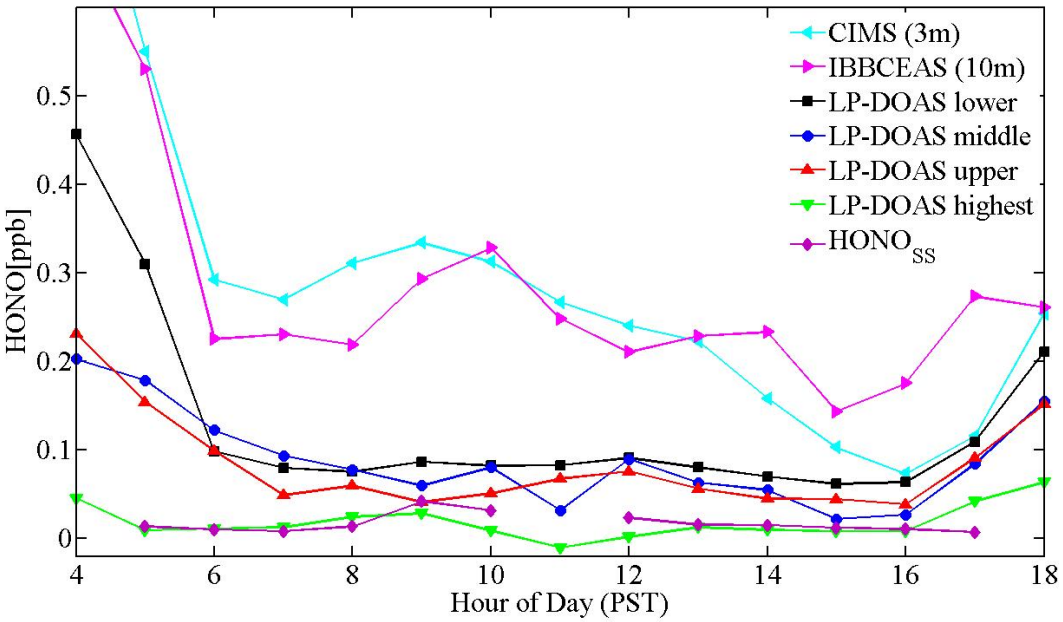

Figure 7.9: Hourly averaged $HONO/NO_2$ ratios calculated from the in-situ instruments at the CalNex-LA site and in the four LP-DOAS height intervals.

7.5 HONO Photolysis as an OH Source

The discussion above focused on the formation of HONO in Los Angeles. An important consequence of the presence of HONO at night and during the day is the formation of OH from the photolysis of HONO. We can distinguish two different impacts. The first is the well-known influence of HONO photolysis in the early morning. Because the photolysis of HONO occurs at longer wavelengths than that of HCHO and O_3, it is often the first OH source in the early morning. The source of this morning HONO is its accumulation in the NBL at night, as described in Section 7.1. Because HONO is restricted to the lowest 50 – 100m in the morning, this source is important for the surface, but most likely less important for the entire daytime boundary layer. Assuming the HONO that accumulated during the night is completely photolyzed during the morning, one can estimate the amount of OH formation from this source. It should be added that it is difficult to provide a representative morning OH formation rate for

the CalNex-LA site as the mountains to the east of the site shadow the site until the sun climbs above the mountain tops. The morning photolysis rates are thus not representative for the entire basin. Nevertheless the assumption of complete photolysis of nocturnal HONO still holds. Using the vertical profiles (Figures 7.2 and 7.3) we calculated the vertically averaged, i.e. in the lowest 550m of the atmosphere, pre-photolysis HONO mixing ratios throughout the CalNex-LA experiment. While the surface HONO levels are often in the range of 0.5 – 2.5 ppb in the morning, this averaged value is much smaller with a campaign averaged value of 0.18 ppb. The temporally integrated OH formation during sunrise is thus 4.5×10^{9} OH molec. cm^{-3}. Assuming a 2 hour sunrise period, this translates to an average morning OH formation rate of 6.25×10^{5} OH molec. cm^{-3} s^{-1} from HONO photolysis in the lowest 550m of the atmosphere. Please note that the formation rate at the surface, which is typically reported in literature, is 10 times higher. However, this rate is not representative for the entire lower atmosphere as discussed above.

HONO later during the day, i.e. daytime HONO, also provides a source for OH. However, its formation is continuous as HONO is formed throughout the day through photo-enhanced reactions. As discussed above, the levels of daytime HONO are significantly higher than the expected photo-stationary state. Consequently HONO photolysis is a net OH source during the day. However, the vertical profile of daytime HONO poses a challenge in the interpretation of the role of HONO as an OH precursor. From Figure 7.8 it is obvious that HONO is a much larger OH source near the surface than aloft, which may skew the assessment of the significance of this source.

To provide a more general assessment of HONO as an OH precursor in Los Angeles we have thus adopted a vertically averaged approach based on our LP-DOAS data, similar to that used in the interpretation of the NO_x budget in Section 6.2. We calculated the OH formation rate from the photolysis of O_3, HONO, and HCHO (assuming that each HO_2 formed is immediately converted into an OH radical by the high levels of NO) for each altitude interval of the LP-DOAS and then integrated these values with altitude. It should be noted that this calculation excludes the lowest 30m of the atmosphere, where HONO is highest. On the other hand, the values integrated from 30-556m are more representative for the polluted boundary layer with respect to the average radical chemistry.

Figure 7.10 shows three days of data for this comparison. We have selected the period from 5/28 to 5/31 when ozone mixing ratios slowly increased from day to day, ending in the highest daytime O_3 mixing ratios during CalNex-LA. It should be added that this period was the Memorial Day weekend from Friday to Sunday and the last two days are thus representative of weekend conditions. On 5/28 the three OH formation pathways discussed here are comparable to each other. One can see that HONO is somewhat more important in the morning, as explained above. The contributions of O_3 and HCHO photolysis increase as the atmosphere in Los Angeles becomes more polluted, while the absolute contribution of HONO remains relatively constant.

This comparison shows that, even considering the vertical profile of HONO and excluding the lowest 30m of the atmosphere, HONO plays a very significant role as a precursor during the day. The accurate description of daytime HONO formation is thus crucial for any air quality model.

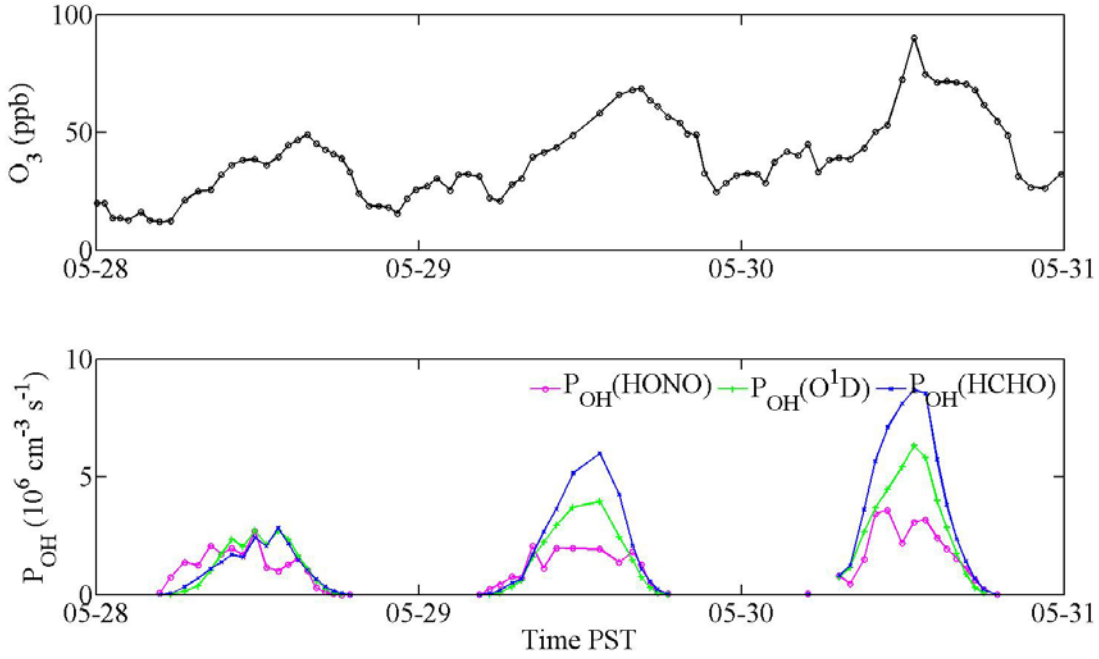

Figure 7.10: OH radical formation rate from O_3 (O_1D), HCHO, and HONO photolysis averaged from 35-556m.

8 Conclusions

The main goal of this project was to investigate the highly altitude dependent nocturnal chemistry in the South Coast Air Basin, with a particular focus on NO_3 chemistry, the nocturnal NO_x budget, and the chemistry of HONO. The following conclusions can be drawn from our study:

Our observations show that nocturnal chemistry in the Los Angeles Basin is highly altitude dependent. The typical diurnal behavior of ozone, i.e. low nocturnal surface mixing ratios, and NO_2, i.e. high nocturnal surface mixing ratios, is mostly restricted to the lower part of the nocturnal boundary layer (NBL). The variation of ozone and NO_2 are much less pronounced aloft. The cause of this behavior is the conversion of ozone to NO_2 through surface emissions of NO. Similar to ozone, the nitrate radical, NO_3, and the related N_2O_5 molecule also show strong vertical profiles with higher mixing ratios aloft. HONO mixing ratios are typically elevated near the surface and decay rapidly with altitude. The vertical trace gas distribution and chemistry is strongly influenced by the magnitude of vertical mixing at night and the NBL height. Any effort to improve the performance of air quality models at night has thus to consider this altitude dependence. A thorough analysis of the nocturnal boundary layer mixing scheme should also be included.

NO_3 mixing ratios in the Los Angeles atmosphere reached above 150 ppt, indicating a very active nocturnal radical chemistry. Most of this oxidative chemistry occurs above the lowest 50m of the atmosphere. N_2O_5, which is related to NO_3 through its equilibrium with NO_2, has high values of up to 2 ppb. Again these values are predominately found above 50 m altitude. The

presence of such high mixing ratios impacts chemistry in multiple ways. NO_3 and N_2O_5 chemistry lead to a destruction of NO_x from the atmosphere (see next point). In addition, O_x is also lost through its NO_3 chemistry. N_2O_5 chemistry also increases aerosol nitrate, thus impacting composition and mass of particulate matter at night. The uptake of N_2O_5 on chloride containing aerosol, which is common in Los Angeles, also leads to the formation of $ClNO_2$, which serves as a radical precursor in the early morning. $ClNO_2$ was observed for the first time in Los Angeles by the University of Calgary. The impact of $ClNO_2$ on Los Angeles air quality needs to be further assessed.

The analysis of our observations allowed us to determine the nocturnal NO_x loss in the Los Angeles atmosphere. It should be noted here that our approach averaged the loss rate over the lowest 550m of the atmosphere. This averaging is critical as the NBL is not well mixed and thus observations at one altitude are not representative for the entire extent of the boundary layer. In the morning when the daytime boundary layer forms, the NBL and the residual layer mix again. The daytime boundary layer was often only 700-800m high during CalNex-LA. Our measurements and analysis thus cover nearly the entire extent of the daytime boundary layer. We identified the aerosol uptake of N_2O_5 as the main loss mechanism for NO_x. Our analysis also revealed that, for the one night of the experiment which we have analyzed in detail, the N_2O_5 uptake coefficient was fairly high, with a value of 0.027. The yield of $ClNO_2$ was found to be around 0.2.

We determined that 0.7 - 1.3 ppb/h of NO_x are lost due to NO_3 chemistry throughout the night in Los Angeles. This NO_x is not available for ozone formation during the next day. To put this NO_x loss into perspective we calculated the loss of NO_x through the OH + NO_2 reaction based on the observations at the CalNex-LA site by the University of Indiana and the University of Houston. For the period we used to determine the nocturnal NO_x loss rate, the average daytime, i.e. from 9:00 to 18:00, NO_x loss was ~0.7 ppb/h. It thus appears that the chemical loss rate of NO_x is comparable between the night and the day. This further emphasizes the need to correctly represent nocturnal NO_3 and N_2O_5 chemistry in urban airshed models.

In collaboration with NOAA we measured detailed vertical profiles of nocturnal HONO during CalNex-LA. These observations show that elevated HONO levels are typically constrained to the lowest 100 m of the atmosphere, although high HONO was also found up to 200 m during a few nights. The profiles are consistent with a conversion of NO_2 to HONO on the surface, followed by slow vertical transport. Our 1-D model is capable of describing the profiles using a simple parameterization based on the reactive uptake of NO_2 on the ground, conversion of NO_2 to HONO on the surface with a yield of 0.5, and a loss of HONO onto the ground. While this approach cannot be used in airshed models, which parameterize the interaction with the surface through deposition velocities and emissions, it may provide guidance on how to develop a better parameterization for nocturnal HONO formation. An accurate description of the mixing and height of the nocturnal boundary layer in airshed models is again crucial to correctly describe nocturnal HONO.

The observations of daytime HONO from the NOAA in-situ instruments as well as UCLA's LP-DOAS system showed the presence of mixing ratios well above the photo-stationary state between OH, NO and HONO. A daytime source of HONO is thus present in Los Angeles. The most likely source is a photo-enhanced surface HONO formation, for example conversion of NO_2 in the presence of surface adsorbed organics. This process would explain the observed vertical HONO profiles and the diurnal variation of the HONO/NO_2 ratio following the

arguments from *Wong et al.* (2001b). Ongoing research will attempt to better quantify this source and to find a parameterization for our 1-D chemistry and transport model, as well as for 3D air chemistry models.

The role of HONO as an OH radical precursor was investigated for the morning photolysis of HONO accumulated during the night, as well as HONO formed during the day. The morning photolysis leads to a substantial OH source near the surface. This confirms earlier findings by *George et.al.* (1999), during the 1993 Los Angeles Free radical study of the importance of HONO as an important early morning OH radical precursor. However, because of the strong vertical profiles of morning HONO, its overall impact is smaller if one considers the vertical extent of the lower atmosphere. We determined an average pre-photolysis HONO mixing ratio of ~0.18 ppb in the lowest 550 m of the Los Angeles atmosphere. One can assume that this entire HONO column is photolyzed in the morning, leading to an average OH formation rate of 6.25×10^5 OH molec. cm^{-3} s^{-1}, assuming a 2 hour period for its photolysis. The peak morning OH formation rate is higher but the shadowing effect of the mountains behind the CalNex-LA site makes this analysis difficult. The contribution of daytime HONO to the OH budget on the other hand is quite substantial, even averaged over the lowest 550m of the atmosphere. For selected days we found that HONO photolysis can be as important as ozone and HCHO photolysis as a precursor of primary OH radical formation. The importance of this contribution varies with pollution levels, i.e. for days with elevated O_3 and HCHO the HONO photolysis contributes less to the overall primary OH formation. The rate of OH formation from daytime HONO photolysis is $\sim2\times10^6$ OH molec. cm^{-3} s^{-1}. At this rate, daytime HONO must be considered in air quality models. It is thus crucial to incorporate daytime HONO formation mechanisms into the models used to simulate the atmospheric chemistry in the Los Angeles Basin.

The previous analysis of the OH budget in Los Angeles during the 1993 Free Radical Study [*Mackay*, 1994, *George et al.*, 1999] did not consider this OH source, and assumed a pure OH + NO $\leftrightarrow$ HONO pseudo steady state. While it is difficult to re-analyze the 1993 observations, the fact that daytime HONO was missing as a source and the good agreements between modeled and observed OH, one can speculate that the OH sinks were also underestimated in the analysis of the 1993 data.

Besides pursuing these goals, UCLA also took the lead in organizing one of the most comprehensive surface measurement sites in California. The site, which was located on the Caltech campus, hosted 40 research groups which deployed over 60 different instruments to provide a complete characterization of the Los Angeles atmosphere. The measurements were made from May 15 to June 16, 2010. The field site was a full success with all instruments being able to perform the planned measurements. The results of these activities have begun to be published in the scientific literature and many more publications from the CalNex-LA site will emerge in the coming years. The data from the field site, including the data presented in this report, are available on a web-site hosted by NOAA.

The results from our project, as well as those from the CalNex-LA field effort, provide the California Air Resources Board and the State of California with an unprecedented view of the atmospheric composition and the chemistry of ozone and particulate matter in the Los Angeles Basin.

9 References

Acker, K., A. Febo, S. Trick, C. Perrino, P. Bruno, P. Wiesen, D. Moller, W. Wieprecht, R. Auel, M. Giusto, A. Geyer, U. Platt, and I. Allegrini (2006a), Nitrous acid in the urban area of Rome, *Atmos. Environ.*, *40*(17), 3123-3133.

Acker, K., D. Moller, W. Wieprecht, F. X. Meixner, B. Bohn, S. Gilge, C. Plass-Dulmer, and H. Berresheim (2006b), Strong daytime production of OH from HNO_2 at a rural mountain site, *Geophys. Res. Lett.*, *33*(2), doi 10.1029/2005gl024643

Acker, K., and D. Moller (2007), Atmospheric variation of nitrous acid at different sites in Europe, *Environ. Chem.*, *4*(4), 242-255.

Alicke, B., A. Geyer, A. Hofzumahaus, F. Holland, S. Konrad, H. W. Patz, J. Schafer, J. Stutz, A. Volz-Thomas, and U. Platt (2003), OH formation by HONO photolysis during the BERLIOZ experiment - art. no. 8247, *J. of Geophys. Res.*, *108*(D4), doi: 10.1029/2001JD000579.

Alicke, B., U. Platt, and J. Stutz (2002), Impact of nitrous acid photolysis on the total hydroxyl radical budget during the Limitation of Oxidant Production/Pianura Padana Produzione di Ozono study in Milan, *J. Geophys. Res.*, *107*(D22), 8196 - doi: 8110.1029/2000JD000075.

Ammann, M., M. Kalberer, D. T. Jost, L. Tobler, E. Rossler, D. Piguet, H. W. Gaggeler, and U. Baltensperger (1998), Heterogeneous production of nitrous acid on soot in polluted air masses, *Nature*, *395*(6698), 157-160.

Aumont, B., F. Chervier, and S. Laval (2003), Contribution of HONO sources to the $NO_x/HO_x/O_3$ chemistry in the polluted boundary layer, *Atmos. Environ.*, *37*(4), 487-498.

Bertram, T., and Thornton, J. (2009). Toward a general parameterization of N_2 O_5 reactivity on aqueous particles: the competing effects of particle liquid water, nitrate and chloride. *Atmos. Chem. Phys*, 9, 8351–8363.

Brown, S. S., H. Stark, T. B. Ryerson, E. J. Williams, D. K. Nicks, M. Trainer, F. C. Fehsenfeld, and A. R. Ravishankara (2003), Nitrogen oxides in the nocturnal boundary layer: Simultaneous in situ measurements of NO_3, N_2O_5, NO_2, NO, and O_3, *J. Geophys. Res.*, *108*(D9), Doi 10.1029/2002jd002917.

Brown, S. S., J. E. Dibb, H. Stark, M. Aldener, M. Vozella, S. Whitlow, E. J. Williams, B. M. Lerner, R. Jakoubek, A. M. Middlebrook, J. A. DeGouw, C. Warneke, P. D. Goldan, W. C. Kuster, W. M. Angevine, D. T. Sueper, P. K. Quinn, T. S. Bates, J. F. Meagher, F. C. Fehsenfeld, and A. R. Ravishankara (2004), Nighttime removal of NOx in the summer marine boundary layer, *Geophys. Res. Lett.*, *31*(7), doi 10.1029/2004gl019412.

Brown, S. S., T. B. Ryerson, A. G. Wollny, C. A. Brock, R. Peltier, A. P. Sullivan, R. J. Weber, W. P. Dube, M. Trainer, J. F. Meagher, F. C. Fehsenfeld, and A. R. Ravishankara (2006), Variability in nocturnal nitrogen oxide processing and its role in regional air quality, *Science*, *311*(5757), 67-70.

Brown, S. S., W. P. Dube, H. D. Osthoff, D. E. Wolfe, W. M. Angevine, and A. R. Ravishankara (2007b), High resolution vertical distributions of NO_3 and N_2O_5 through the nocturnal boundary layer, *Atmos. Chem. Phys.*, *7*, 139-149.

Brown, S. S., W. P. Dube, H. D. Osthoff, J. Stutz, T. B. Ryerson, A. G. Wollny, C. A. Brock, C. Warneke, J. A. De Gouw, E. Atlas, J. A. Neuman, J. S. Holloway, B. M. Lerner, E. J. Williams, W. C. Kuster, P. D. Goldan, W. M. Angevine, M. Trainer, F. C. Fehsenfeld, and A. R. Ravishankara (2007a), Vertical profiles in NO_3 and N_2O_5 measured from an aircraft: Results from the NOAA P-3 and surface platforms during the New England Air Quality Study 2004, *J. Geophys. Res.*, *112*(D22), Doi 10.1029/2007jd008883.

Calvert, J. G., G. Yarwood, and A. M. Dunker (1994), An Evaluation of the Mechanism of Nitrous Acid Formation in the Urban Atmosphere, *Res. Chem. Inter.*, *20*(3-5), 463-502.

Dentener, F. J., and P. J. Crutzen (1993), Reaction of N_2O_5 on tropospheric aerosols: Impact on the global distributions of NO_x, O_3, and OH, *J. Geophys. Res.*, *98*(D4), 7149-7163.

Docherty, K. S., and P. J. Ziemann (2006), Reaction of oleic acid particles with NO_3 radicals: Products, mechanism, and implications for radical-initiated organic aerosol oxidation, *J. Phys. Chem. A*, *110*(10), 3567-3577.

Finlayson- Pitts, B. J., L. M. Wingen, A. L. Sumner, D. Syomin, and K. A. Ramazan (2003), The heterogeneous hydrolysis of NO_2 in laboratory systems and in outdoor and indoor atmospheres: An integrated mechanism, *Phys. Chem. Chem. Phys.*, *5*, 223-242.

Gerecke, A., A. Thielmann, L. Gutzwiller, and M. J. Rossi (1998), The chemical kinetics of HONO formation resulting from heterogeneous interaction of NO_2 with flame soot, *Geophys. Res. Lett. (USA)*, *25*, 2453-2456.

Geyer, A., and J. Stutz (2004), Vertical profiles of NO_3, N_2O_5, O_3, and NO_x in the nocturnal boundary layer: 2. Model studies on the altitude dependence of composition and chemistry, *J. Geophys. Res.*, *109*(D12), Doi 10.1029/2004jd005217.

Geyer, A., B. Alicke, R. Ackermann, M. Martinez, H. Harder, W. Brune, P. di Carlo, E. Williams, T. Jobson, S. Hall, R. Shetter, and J. Stutz (2003), Direct observations of daytime NO3: Implications for urban boundary layer chemistry, *J. Geophys. Res.*, *108*(D12), doi 10.1029/2002jd002967.

George L. A., Hard T.M., O'Brien R.J. (1999), Measurements of free radicals OH and HO_2 in Los Angeles smog, *J. Geophys. Res.*, *104*(D09), doi 10.1029/1998JD100113.

Goodman, A. L., G. M. Underwood, and V. H. Grassian (1999), Heterogeneous reaction of NO_2: Characterization of gas-phase and adsorbed products from the reaction, $2NO_{(2)}(g)+H_2O(a)$-> $HONO(g)+HNO_3(a)$ on hydrated silica particles, *J. Phys. Chem. A*, *103*(36), 7217-7223.

Grannas, A. M., Jones A.E., Dobb J., Ammann M., Anastasio C., Beine H.J., Bergin M., Bottenheim J., Boxe C.S., Carver G., Chen G., Crawford G.H., Domin´e F., and Zhu T.(2007), An overview of snow photochemistry: evidence, mechanisms and impacts, *Atmos. Chem. Phys.*, *7*(16), 4329-4373.

Haman, C. L., Lefer, B., Morris, G. A. (2012). Seasonal Variability in the Diurnal Evolution of the Boundary Layer in a Near Coastal Urban Environment. *J. Atmos. Ocean. Techn.*, 120209142339000. doi:10.1175/JTECH-D-11-00114.1

Harris, G. W., W. P. L. Carter, A. M. Winer, J. N. Pitts, U. Platt, and D. Perner (1982), Observations of nitrous acid in the Los Angeles atmosphere and implications for the predictions of ozone-precursor relationships, *Environ. Sci. Technol.*, *16*, 414-419.

Harris, G.W., et al., Measurement of HONO, NO_3 and NO_2 by long-path differential optical absorption spectroscopy in the Los Angeles basin (1983), in *Optical and Laser Remote Sensing*, *Springer Ser. Opt. Sci.*, *39*, 106-113.

Hu, J.H., Abbatt, J.P.D., (1997), Reaction probabilities for N_2O_5 hydrolysis on sulfuric acid and ammonium sulfate aerosols at room temperature. *J. Phys Chem. A*, 101, 871–878.

Jacob, D.J. (2000), Heterogeneous chemistry and tropospheric ozone. *Atmospheric Environment* 34, 2131e2159.

Jenkin, M. I., R. A. Cox, and D. J. Williams (1988), Laboratory studies of the kinetics of formation of nitrous acid from the thermal reaction of nitrogen dioxide and water vapour, *Atmos. Environ.*, *22*, 487-498.

Kalberer, M., M. Ammann, F. Arens, H. W. Gaggeler, and U. Baltensperger (1999), Heterogeneous formation of nitrous acid (HONO) on soot aerosol particles, *J Geophys Res.*, *104*(D11), 13825-13832.

Kane, S. M., F. Caloz, and M. T. Leu (2001), Heterogeneous uptake of gaseous N_2O_5 by $(NH_4)_2SO_4$, NH_4HSO_4, and H_2SO_4 aerosols, *J. Phys. Chem. A*, *105*(26), 6465-6470.

Karagulian, F., and M. J. Rossi (2007), Heterogeneous chemistry of the NO_3 free radical and N_2O_5 on decane flame soot at ambient temperature: Reaction products and kinetics, *J. Phys. Chem. A*, *111*(10), 1914-1926.

Kirchstetter, T. W., R. A. Harley, and D. Littlejohn (1996), Measurement of Nitrous Acid in Motor Vehicle Exhaust, *Environ Sci Technol*, *30*(9), 2843-2849.

Kleffmann, J. (2007), Daytime sources of nitrous acid (HONO) in the atmospheric boundary layer, *Chem. Phys. Phys. Chem.*, *8*(8), 1137-1144.

Kleffmann, J., J. C. Lorzer, P. Wiesen, C. Kern, S. Trick, R. Volkamer, M. Rodenas, and K. Wirtz (2006), Intercomparison of the DOAS and LOPAP techniques for the detection of nitrous acid (HONO), *Atmos. Environ.*, *40*(20), 3640-3652.

Kleffmann, J., K. H. Becker, and P. Wiesen (1998), Heterogeneous NO_2 conversion processes on acid surfaces: possible atmospheric implications, *Atmos. Environ.*, *32*, 2721 - 2729.

Kurtenbach, R., K. H. Becker, J. A. G. Gomes, J. Kleffmann, J. C. Lorzer, M. Spittler, P. Wiesen, R. Ackermann, A. Geyer, and U. Platt (2001), Investigations of emissions and heterogeneous formation of HONO in a road traffic tunnel, *Atmos. Environ.*, *35*(20), 3385-3394.

Lammel, G., and J. N. Cape (1996), Nitrous acid and nitrite in the atmosphere, *Chem Soc Rev*, *25*(5), 361+.

Landgraf, J., and P. Crutzen (1998), An efficient method for 'on-line' calculations of photolysis and heating rates, *J. Atmos. Sci.*, 55, 863– 878.

Li, S. P., J. Matthews, and A. Sinha (2008), Atmospheric hydroxyl radical production from electronically excited NO_2 and H_2O, *Science*, *319*(5870), 1657-1660.

Mackay G. I. (1994), Claremont Atmospheric Free-Radical Study: Measurements of formaldehyde, hydrogen peroxide, nitric acid, nitrous acid, peroxyacetyl nitrate, nitrogen dioxide, nitrogen oxides, ozone, carbon monoxide, hydrocarbons (C_1-C_{12}) and carbonyl compounds (C_1-benzaldehyde), Final Report to the California Air Resources Board, Sacramento No. 92-327.

Mak, J., S. Gross, and A. K. Bertram (2007), Uptake of NO_3 on soot and pyrene surfaces, *Geophys. Res. Lett.*, *34*(10), doi 10.1029/2006gl029756.

Meller R., Moorgat G.K. (2000), Temperature dependence of absorption cross sections of formaldehyde between 223 and 323 K in the wavelength range 225-375 nm, *J. Geosphys. Res.*, 105(D6), 7089-7101.

Michel, A.E., Usher, C.R., Grassian, V.H., (2002), Heterogeneous and catalytic uptake of ozone on mineral oxides and dusts: a Knudsen cell investigation. *Geophy. Res. Lett.*, 29, 1665, doi:10.1029/2002GL014896.

Osthoff, H. D., R. Sommariva, T. Baynard, A. Pettersson, E. J. Williams, B. M. Lerner, J. M. Roberts, H. Stark, P. D. Goldan, W. C. Kuster, T. S. Bates, D. Coffman, A. R. Ravishankara, and S. S. Brown (2006), Observation of daytime N_2O_5 in the marine boundary layer during New England Air Quality Study - Intercontinental Transport and Chemical Transformation 2004, *J Geophys.l Res.*, *111*(D23), Doi 10.1029/2006jd007593.

Osthoff, H. D., Roberts, J. M., Ravishankara, a. R., Williams, E. J., Lerner, B. M., Sommariva, R., Bates, T. S., et al. (2008). High levels of nitryl chloride in the polluted subtropical marine boundary layer. Nature Geoscience, 1(5), 324-328. doi:10.1038/ngeo177

Perner, D., and U. Platt (1979), Detection of Nitrous-Acid in the Atmosphere by Differential Optical-Absorption, *Geophys. Res. Lett.*, *6*(12), 917-920.

Pitts, J. N., H. W. Biermann, A. M. Winer, E. C. Tuazon, M. (1984a), Spectroscopic identification and measurement of gaseous nitrous acid in dilute auto exhaust, *Atmos. Environ.*, *18*, 847-854.

Pitts, J. N., E. Sanhueza, R. Atkinson, W. P. L. Carter, A. M. Winer, G. W. Harris, and C. N. Plum (1984b), An investigation of the dark formation of nitrous acid in environmental chambers, *Int. J. Chem. Kinet.*, *XVI*, 919-939.

Platt, U., and D. Perner (1980), Direct measurements of atmospheric CH_2O, HNO_2, O_3, NO_2, and SO_2 by differential optical absorption in the near UV, *J. Geophys. Res.*, *85*, 7453-7458.

Platt, U., A. Winer, H. Biermann, R. Atkinson, and J. Pitts, JN (1984), Measurement of nitrate radical concentration in continental air, *Env. Sci. Techn.*, *18*, 365 - 369.

Platt, U. and J. Stutz (2008), *Differential Optical Absorption Spectroscopy: Principles and Applications*, Springer Verlag, Heidelberg, 597pp.

Ren, X. R., et al. (2006), Behavior of OH and HO_2 in the winter atmosphere in New York city, *Atmos. Environ.*, *40*, S252-S263.

Rudich, Y., Talukdar, R.K., Ravishankara, A.R., Fox, R.W., (1996), Reactive uptake of NO_3 on pure water and ionic solutions. Journal of Geophysical Research 101, 21023–21031.

Sakamaki, F., S. Hatakeyama, and H. Akimoto (1983), Formation of nitrous acid and nitric oxide in the heterogeneous dark reaction of nitrogen dioxide and water vapor in a smog chamber, *Int. J. Chem. Kinet.*, *XV*, 1013-1029.

Saliba, N. A., M. Mochida, and B. J. Finlayson-Pitts (2000), Laboratory studies of sources of HONO in polluted urban atmospheres, *Geophys. Res. Lett.*, *27*(19), 3229-3232.

Sander S.P., R.R. Friedl, J.R. Barker, D.M. Golden, M.J. Kurylo, P.H. Wine, J.P.D. Abbatt, J.B. Burkholder, C.E. Kolb, G.K. Moortgat, R.E. Huie, V.L., Orkin (2011), Chemical Kinetics and Photochemical Data for Use in Atmospheric Studies, Evaluation Number 17, JPL Publication 10-6.

Shetter and Muller (1999), Photolysis frequency measurements using actinic flux spectroradiometry during the PEM-Tropics mission: Instrumentation description and some results, *J. Geophys. Res.*, 104 (D5), 5647-5661, doi:10.1029/98JD01381

Sjödin, A., and M. Ferm (1985), Measurement of nitrous acid in an urban area, *Atmos. Environ.*, *19*, 985-992.

Stark, H., S. S. Brown, K. W. Wong, J. Stutz, C. D. Elvidge, I. B. Pollack, T. B. Ryerson, et al. (2011). City lights and urban air. *Nature Geoscience*, 4(11), 730-731. doi:10.1038/ngeo1300.

Stemmler, K., M. Ndour, Y. Elshorbany, J. Kleffmann, B. D'Anna, C. George, B. Bohn, and M. Ammann (2007), Light induced conversion of nitrogen dioxide into nitrous acid on submicron humic acid aerosol, *Atmos Chem. Phys.*, *7*(16), 4237-4248.

Stockwell, W. R., F. Kirchner, M. Kuhn and S. Seefeld (1997), A new mechanism for regional atmospheric chemistry modeling, J. Geophys. Res., 102 (D22), 25847-25879.

Stutz, J., Kim, E.S., Platt, U., Bruno, P., Perrino, C., Febo, A., (2000), UV-Visible absorption cross section of nitrous acid, J. Geophys. Res. 105 (D11), 14585–14592.

Stutz, J., B. Alicke, R. Ackermann, A. Geyer, A. White, and E. Williams (2004a), Vertical profiles of NO_3, N_2O_5, O_3, and NO_x in the nocturnal boundary layer: 1. Observations during the Texas Air Quality Study 2000, *J. Geophys. Res.*, *109*(D12), doi 10.1029/2004jd005216.

Stutz, J., B. Alicke, R. Ackermann, A. Geyer, S. Wang, A. White, E. Williams, C. Spicer, and J. D. Fast (2004b), Relative humidity dependence of HONO chemistry in urban areas, *J. Geophys. Res.*, *109*(D3), doi 10.1029/2003jd004135.

Stutz, J., Wong, K.W., Lawrence, L., Ziemba, L., Flynn, J.H., Rappenglück, and B., Lefer (2010), Nocturnal NO_3 radical chemistry in Houston, TX, *Atmos. Environ.*, 44, 4099-4106, doi: 10.1016/j.atmosenv.2009.03.004.

Svensson, R., E. Ljungström, and O. Lindqvist (1987), Kinetics of the reaction between nitrogen dioxide and water vapour, *Atmos. Environ.*, *21*, 1529-1539.

Thornton, J. A., and J. P. D. Abbatt (2005), N_2O_5 reaction on submicron sea salt aerosol: Kinetics, products, and the effect of surface active organics, *J. of Phys. Chem. A*, *109*(44), 10004-10012.

Thornton, J. A., C. F. Braban, and J. P. D. Abbatt (2003), N_2O_5 hydrolysis on sub-micron organic aerosols: the effect of relative humidity, particle phase, and particle size, *Phys. Chem. Chem. Phys.*, *5*(20), 4593-4603.

Trick, S., Formation of nitrous acid on urban surfaces – a physical-chemical perspective, PhD thesis University of Heidelberg, Heidelberg, Germany, 2004.

Vandaele, A. C., P. C. Simon, J. M. Guilmot, M. Carleer, and R. Colin (1994), SO_2 absorption cross section measurement in the UV using a Fourier transform spectrometer, J. Geophys. Res., 99, 25,599–25,605.

Veres P., J. M. Roberts, C. Warneke, D. Welsh-Bon, M. Zahniser, S. Herndon, R. Fall, J. de Gouw, (2008), Development of negative-ion proton-transfer chemical-ionization mass spectrometry (NI-PT-CIMS) for the measurement of gas-phase organic acids in the atmosphere, *Int. J. Mass Spectr*., 274, 48-55, doi: 10.1016/j.ijms.2008.04.032.

Voigt, S., J. Orphal, K. Bogumil, and J. P. Burrows (2001), The temperature dependence (203-293 K) of the absorption cross sections of O3 in the 230-850 nm region measured by Fourier-transform spectroscopy, J. Photochem and Photobiol. A, 143, 1-9.

Voigt, S., J. Orphal, and J. P. Burrows (2002), The temperature and pressure dependence of the absorption cross-sections of NO_2 in the 250-800 nm region measured by Fourier-transform spectroscopy, J Photochem Photobiol a, 149, 1-7.

Wang, S., R. Ackermann, and J. Stutz (2006), Vertical profiles of O_3 and NO_x chemistry in the polluted nocturnal boundary layer in Phoenix, AZ: I. Field observations by long-path DOAS, *Atmos. Chem. Phys.*, *6*, 2671-2693.

Washenfelder, R., Langford, A., Fuchs, H., and Brown, S. (2008). Measurement of glyoxal using an incoherent broadband cavity enhanced absorption spectrometer. *Atm. Chem. Phys.*, *8*, 16517–16553.

Wayne, R.P., I. Barnes, P. Biggs, J.P. Burrows, C.E. Canosa-Mas, J. Hjorth, G. Le Bras, G. Moortgat, D. Perner, G. Poulet, G. Restelli, and H. Sidebottom (1991), The nitrate radical: Physics, chemistry, and the atmosphere, *Atmos. Environ.*, *25A*, 1-203.

Winer, A. M., and H. W. Biermann (1994), Long Pathlength Differential Optical Absorption Spectroscopy (DOAS) Measurements of Gaseous HONO, NO_2 and HCHO in the California South Coast Air Basin, *Res Chem Interm.*, *20*(3-5), 423-445.

Wong, K. W. , H.-J. Oh, B. Lefer, B. Rappenglück, and J. Stutz (2011a) Vertical profiles of nitrous acid in the nocturnal urban atmosphere of Houston, TX, *Atmos. Chem. Phys.*, 11, 3595-3609, doi: 10.5194/acp-11-3595-2011.

Wong, K. W., C. Tsai, B. Lefer, C. Haman, N. Grossberg, W. H. Brune, X. Ren, W. Luke, and J. Stutz (2011b), Daytime HONO Vertical Gradients during SHARP 2009 in Houston, TX, *Atmos. Chem. Phys. Discuss.*, 11, 24365-24411.

Yokelson, R., Burkholder, J., Fox, R., Talukdar, R., Ravishankara, A., (1994). Temperature dependence of the NO_3 absorption spectrum. *J. Phys. Chem. A* 98, 13144–13150.

Zhou, X. L., Y. He, G. Huang, T. D. Thornberry, M. A. Carroll, and S. B. Bertman (2002), Photochemical production of nitrous acid on glass sample manifold surface, *Geophys. Res. Lett.*, *29*(14), doi 10.1029/2002gl015080.

10 Glossary of Terms, Abbreviations and Symbols

BLH – boundary layer height
CAPS - Cavity attenuated phase shift
CEAS-DOAS - Cavity Enhanced Absorption Spectroscopy Differential Optical Absorption Spectroscopy
CIMS - Chemical Ionization Mass Spectrometry
GC-MS – Gas chromatography – Mass spectrometry
IBBCEAS - Incoherent Broadband Cavity Enhanced Absorption Spectrometer
QC-TILDAS - Quantum Cascade Tunable Infrared Laser Differential Absorption Spectrometer
DOAS – Differential Optical Absorption Spectroscopy
LIF-FAGE - laser induced fluorescence
LP-DOAS – longpath Differential Optical Absorption Spectroscopy
MAX-DOAS – Multi-Axis Differential Optical Absorption Spectroscopy
NOAA – National Oceanic and Atmospheric Administration
NOAA ARL - National Oceanic and Atmospheric Administration Air Resources Laboratory
PALMS - Particle Analysis by Laser Mass Spectrometry
PAM – potential aerosol mass
PILS – particle-into-liquid sampler
PM – particulate matter
TAG-AMS - Thermal desorption Aerosol GC - Aerosol Mass Spectrometer
TSI SMPS – Scanning Mobility Particle Sizer
UCLA – University of California Los Angeles
UHSAS - Ultra-High Sensitivity Aerosol Spectrometer